/ CERN PRE 93-080

ERICE PREPRINT SERIES

SW 9406

«ETTORE MAJORANA» CENTRE FOR SCIENTIFIC CULTURE

EMCSC/93-08
20 December 1993

INTRINSIC CHARM IN pp AND γp INTERACTIONS

G. Anzivino[4], F. Arzarello[2], G. Bari[2], M. Basile[2,7], L. Bellagamba[2], D. Boscherini[2], G. Bruni[2], P. Bruni[2], G. Cara Romeo[2], M. Chiarini[2,11], L. Cifarelli[2,8], F. Cindolo[2], F. Ciralli[2], A. Contin[1,2], M. Dardo[5,10] S. D'Auria[2], C. Del Papa[2,7], S. De Pasquale[4], F. Frasconi[2], P. Giusti[2], G. Iacobucci[2], G. Maccarrone[4], A. Margotti[2], T. Massam[2], R. Nania[2], H. I. Petrache[3,11], S. Qian[2,11], G. Sartorelli[2,7], Yu. M. Shabelski[3,9,11], M. A. Stepanov[3,9,11], O. P. Strogova[3,6,11], R. Timellini[2,11], L. Votano[4] and A. Zichichi[1,2]

1) CERN, Geneva, Switzerland
2) INFN, Bologna, Italy
3) INFN, Eloisatron Project, Erice, Italy
4) INFN, LNF, Frascati, Italy
5) INFN, Torino, Italy
6) INP, Moscow State University, Moscow, Russia
7) Physics Department, University of Bologna, Italy
8) Physics Department, University of Pisa, Italy
9) PNPI, Gatchina, St. Petersburg, Russia
10) II Faculty of Science, University of Torino, Alessandria, Italy
11) World Laboratory, Lausanne, Switzerland

Abstract

In the Parton Fusion Model (PFM) the intrinsic charm (IC) mechanism can induce a significant contribution to the differential cross-sections of charmed hadrons at large Feynman-x in pp collisions. The possibility to include the intrinsic charm component in the Quark-Gluon String Model (QGSM) is also presented and the results from the two models are compared with each other and with the existing experimental data on D, $\overline{D}$ and Λ_c hadroproduction. In connection with HERA experiments, the effects of intrinsic charm as predicted by PFM in high energy photoproduction are carefully investigated.

(Submitted to Il Nuovo Cimento)

EMCSC - Via Guarnotta 26 - 91016 Erice - Italy - Tel. (923) 869133 - Fax. (923) 869226

1. INTRODUCTION

The Parton Fusion Model (PFM) [1] may be used to predict heavy quark production in hadron-hadron collisions or in lepton-hadron deep inelastic scattering (DIS). Many calculations have been made using different parton structure functions in the proton and the results have clearly shown their dependence not only on structure functions but also on the QCD scale Q^2 and coupling α_s. However a common characteristic is that all the differential cross-sections of charmed hadrons given by PFM decrease at large x_F (Feynman-x) more rapidly than the experimental ones. Beside the need to learn more about the parton structure functions, it is worth searching for other possible mechanisms to be added to PFM. The possibility to account for the difference between the experimental data and model predictions at large x_F using the intrinsic charm (IC) mechanism [2-5] comes from the fact that the $c\bar{c}$ pair can be a component of the proton wave-function. In this case the charmed quarks would carry a larger fraction of the proton momentum than the other components, because the velocities of all quarks are assumed to be the same [2].

According to the intrinsic quark hypothesis, there are heavy quark pairs in a proton which are freed in hadronic collisions via soft interactions of light quarks. The corresponding cross-section is expressed as [2]:

$$\frac{d\sigma_{IC}}{dx_1...dx_n} = N_n \cdot \frac{\delta(1-\sum_{i=1}^{n} x_i)}{(m_p^2 - \sum_{i=1}^{n} \frac{\hat{m}_\perp^2}{x_i})^2}, \tag{1}$$

where N_n is a normalization factor, m_p the proton mass, x_i the fraction of initial proton momentum carried by a component i, $\hat{m}_i = (m_i^2 + < \vec{k}_{\perp i}^2 >)^{1/2}$ its transverse mass and n the total number of components (valence plus intrinsic quarks) in a proton.

For charm quarks the Fock-state decomposition of the proton wave-function is assumed to be:

$$|p> = \alpha \cdot |uud> + \beta \cdot |uudc\bar{c}> + ..., \tag{2}$$

with a small β^2 probability of finding a $c\bar{c}$ pair.

IC effects can also be considered in the framework of the Quark-Gluon String Model (QGSM) [6]. This model is a version of the Dual Topological Unitarization (DTU) approach of QCD and describes many features of multiparticle production processes in high-energy hadron collisions, such as the inclusive spectra of different secondary hadrons, their multiplicities, KNO-distributions, etc. High-energy soft interactions are considered in this case as proceeding via one or several pomeron exchanges and described by cylindrical-type diagrams. Every cylinder, whose surface represents a net of gluons and quark-antiquark pairs, corresponds to a one-pomeron exchange. The relative contribution of multipomeron diagrams increases with the energy. All elastic and diffractive processes with multipomeron exchanges are the results of cuts between pomerons, while all inelastic processes are obtained by cutting one or several pomerons [7], see fig. 1. QGSM predictions for the inclusive spectra of heavy-flavoured hadrons were considered earlier (without intrinsic charm) in [8-10].

In the present paper we study the effects of intrinsic charm in PFM (sect. 2) and in QGSM (sect. 3) as far as pp interactions are concerned. The two approaches are compared with each other and with the existing experimental data in sect. 4. Then we apply the PFM plus IC formalism to γp interactions at different energies, having in mind the real or quasi-real photoproduction of heavy flavours at HERA. A discussion of the results and our concluding remarks are given in sect. 6.

2. INTRINSIC CHARM CONTRIBUTION TO HADROPRODUCTION IN PFM

In PFM the cross-section for the production of heavy quark pairs $Q\overline{Q}$ in the interaction of hadrons A and B, at a squared center-of-mass energy $s = (p_A + p_B)^2$, is:

$$\sigma^{AB\to Q\overline{Q}} = \int_{x_{a0}}^{1} \frac{dx_a}{x_a} \int_{x_{b0}}^{1} \frac{dx_b}{x_b} \left[x_a G_{a/A}(x_a, Q^2)\right] \left[x_b G_{b/B}(x_b, Q^2)\right] \hat{\sigma}^{ab\to Q\overline{Q}}(\hat{s}, m_Q, Q^2), \quad (3)$$

where $x_{a0} = 4m_Q^2/s$ and $x_{b0} = 4m_Q^2/sx_a$. Here $G_{a/A}(x_a, Q^2)$ and $G_{b/B}(x_b, Q^2)$ are the structure functions of partons a and b inside hadrons A and B, respectively, and $\hat{\sigma}^{ab\to Q\overline{Q}}(\hat{s}, m_Q, Q^2)$ is the cross-section for the subprocess $ab \to Q\overline{Q}$ as given by standard QCD [11]. The latter depends on the parton center-of-mass energy $\hat{s} = (p_a + p_b)^2 = x_a x_b s$, the mass of the produced heavy quark m_Q, and the QCD scale Q^2. Equation (3) should account for all possible subprocesses $ab \to Q\overline{Q}$.

The resulting total cross-sections for charm production in pp interactions at three different energies (p_{lab} = 200, 400 and 800 GeV/c) are presented in table 1. The PFM values obtained using MT (S-DIS) parton structure functions [12], with Q^2 = 4 GeV^2, are near to the lower boundary of the corresponding experimental measurements, also presented in table 1.

Let us introduce now the contribution from IC mechanism. In accordance with (1), the inclusive cross-section for charm quark production is equal to:

$$\frac{d\sigma_{IC}}{dx_c} = \int \frac{d\sigma_{IC}}{dx_1 dx_2 dx_3 dx_c dx_{\overline{c}}} dx_1 dx_2 dx_3 dx_{\overline{c}}, \quad (4)$$

where the subscripts 1 to 3 refer to the proton valence quarks (uud). The values used in [2] for the transverse masses are $\hat{m}_q$ = 0.45 GeV for light quarks and $\hat{m}_c$ = 1.8 GeV for charmed quarks.

Charmed quarks fragment into charmed hadrons thus transferring a fraction $z = |\vec{p}_H|/|\vec{p}_c|$ of their momentum. This process can be described with the help of Peterson fragmentation function [15]:

$$D_{H/c}(z) = \frac{N}{z\left(1 - \frac{1}{z} - \frac{\epsilon_c}{1-z}\right)^2}. \quad (5)$$

where N is a normalization factor and ϵ_c a parameter defined in [15] as:

$$\epsilon_c = (\frac{m_q}{m_c})^2 \approx 0.06. \quad (6)$$

The cross-section for charmed hadron production has the form:

$$\frac{d\sigma_{IC}}{dx_H} = \int \frac{d\sigma_{IC}}{dx_c} D_{H/c}(z)\delta(x_H - zx_c)\, dx_c dz = \int_{x_H}^{1} \left(\left.\frac{d\sigma_{IC}}{dx_c}\right|_{x_c=\frac{x_H}{z}} \right) \frac{D_{H/c}(z)}{z} dz. \quad (7)$$

The distributions (4) and (7), normalized to unity, for intrinsic c quarks fragmenting into charmed hadrons are presented in fig. 2. Peterson fragmentation causes a decrease of the average momentum, as expected. Notice that the curves of fig. 2 are the same for inrinsic c or $\bar{c}$ quarks.

The dominant channels for charmed hadron production are $D\overline{D}$ and $\Lambda_c\overline{D}$. Studies of Λ_c production in pp interactions at $p_{lab} = 400$ GeV/c [13] show that $\sigma(\Lambda_c\overline{D}) < \sigma(D\overline{D})$ and following [2] we assume:

$$\sigma(\Lambda_c) = \frac{1}{3}\sigma_{tot}^{pp\to c\bar{c}}, \ \sigma(D) = \frac{2}{3}\sigma_{tot}^{pp\to c\bar{c}}, \ \sigma(\overline{D}) = \sigma_{tot}^{pp\to c\bar{c}}, \tag{8}$$

where $\sigma_{tot}^{pp\to c\bar{c}}$ is the total $c\bar{c}$ production cross-section.

The cross-section for charm production via IC mechanism has a very weak energy dependence (the same as σ_{inel}^{pp}), as compared to the corresponding PF cross-section. So the effects of IC in pp collisions should mostly appear at moderately high energies. For numerical calculations it is necessary to normalize the IC contribution to the PF one (i.e. to determine the value of β in eq. (2)).

In [2] the ratio of intrinsic charm cross-section to total charm cross-section in pp collisions at $p_{lab} = 200$ GeV/c was proposed to be:

$$\frac{\sigma_{IC}}{\sigma_{tot}^{pp\to c\bar{c}}} = 0.11. \tag{9}$$

Using the value of $\sigma_{PF}^{pp\to c\bar{c}}$ at the same energy (table 1), the above ratio (9) gives $\sigma_{IC} \approx 0.6$ μb. This contribution of intrinsic charm to the total cross-section is not significant and it is several times smaller than the differences between PF calculations obtained with different types of parton structure functions [16].

3. INTRINSIC CHARM CONTRIBUTION TO HADROPRODUCTION IN QGSM

As previously mentioned, high-energy hadronic interactions are considered in QGSM as proceeding via the exchange of one or several pomerons. Each pomeron corresponds to a cylindrical diagram so in the case of a pomeron cut two showers of secondaries are produced (see fig. 1). The inclusive spectra of secondaries are determined by the convolutions of diquark, valence and sea quark distributions $u(x,n)$ in the incident particles with quark and diquark fragmentation functions into secondary hadrons $G(z)$. The diquark and quark distribution functions depend on the number n of cut pomerons in the considered diagrams. The inclusive spectrum of a secondary hadron h has the form [6]:

$$1/\sigma_{inel} \cdot d\sigma/dx = \sum_{n=1}^{\infty} w_n \phi_n^h(x) + V_D^{(1)}\phi_D^{(1)}(x) + V_D^{(2)}\phi_D^{(2)}(x). \tag{10}$$

where the functions $\phi_n^h(x)$ determine the contributions of diagrams with n cut pomerons and the factors w_n are the probabilities of these processes. The last two terms in eq. (10) account for the contributions of diffraction-dissociation processes and they are negligibly small for charmed hadron production.

In the case of pp collisions:

$$\phi_n^h(x) = f_{qq}^h(x_+, n) f_q^h(x_-, n) + f_q^h(x_+, n) f_{qq}^h(x_-, n) + 2(n-1) f_s^h(x_+, n) f_s^h(x_-, n), \quad (11)$$

with

$$x_\pm = \frac{1}{2}[\sqrt{4m_T^2/s + x^2} \pm x], \quad (12)$$

where m_T is the usual transverse mass of the hadron. The functions f_{qq}, f_q and f_s correspond to the contributions of diquarks, valence and sea quarks, respectively. They are determined by the convolutions of diquark and quark distributions with fragmentation functions, e. g.:

$$f_q^h(x_+, n) = \int_{x_+}^1 u_q(x_1, n) G_q^h(x_+/x_1) dx_1. \quad (13)$$

In the present calculations we use the quark and diquark distributions of the proton in the form [6]:

$$\begin{aligned} u_{uu}(x, n) &= C_{uu} x^{2.5} (1-x)^{n-1.5}, \\ u_{ud}(x, n) &= C_{ud} x^{1.5} (1-x)^{n-1.5}, \\ u_u(x, n) &= C_u x^{-0.5} (1-x)^{n+0.5}, \\ u_d(x, n) &= C_d x^{-0.5} (1-x)^{n+1.5}, \end{aligned} \quad (14)$$

$$u_{\overline{u}}(x, n) = u_{\overline{d}}(x, n) = C_{\overline{u}} x^{-0.5} [(1+\delta/2)(1-x)^{n+0.5}(1-x/3) - \delta/2(1-x)^{n+1}] \ , \ n > 1,$$

$$u_s(x, n) = C_s x^{-0.5} (1-x)^{n+1} \ , \ n > 1, \quad (15)$$

where $\delta = \delta_s + \delta_c$, δ_s and δ_c being the relative probabilities to find a strange and a charmed quark in the sea. These are assumed to be:

$$\delta_s = 0.2 \ , \ \delta_c = 0.04. \quad (16)$$

The ratio $\delta_c : \delta_s = 1 : 5$ may be considered as unexpectedly large, however in QGSM at moderate energies ($\sqrt{s} = 20 \div 30$ GeV) strange hadrons are mostly produced via the fragmentation of u and d quarks and diquarks and only about 1% via the fragmentation of s and $\overline{s}$ quarks. At $p_{lab} = 200$ GeV/c the value $\delta_c = 0.04$ leads to an IC cross-section equal to 0.6 μb, as in [2].

The factors C_i and C_{ij} in eqs. (14) and (15) are determined from the condition:

$$\int_0^1 u_{i(ij)}(x, n) dx = 1. \quad (17)$$

To account for the IC contribution we assume that there are $c\overline{c}$ pairs in the sea and that charm quarks have the same x-distribution as strange quarks:

$$u_c(x, n) = C_c x^{-0.5} (1-x)^{n+1} \ , \ n > 1. \quad (18)$$

Then we consider the $f_s^h(x_+, n)$ and $f_s^h(x_-, n)$ contributions in eq. (11) as the sum of four terms:

$$f_s^h = \frac{1}{2 + \delta_s + \delta_c} [f_{\overline{u}}^h + f_{\overline{d}}^h + \delta_s f_{\overline{s}}^h + \delta_c f_{\overline{c}}^h]. \quad (19)$$

Such an assumption is in some disagreement with the intrinsic charm hypothesis because c and $\bar{c}$ quarks should rather be considered as valence quarks. However in this case we should consider new kinds of strings: between $(qc\bar{c})$ and qq, and between $(qqc\bar{c})$ and q, where q and qq are the usual quark and diquark inside the proton. The fragmentation functions of the new objects $(qc\bar{c})$ and $(qqc\bar{c})$ are unknown, so our results will depend on the assumptions about these functions. Nevertheless the inclusive spectra of secondary charmed hadrons mainly depend on the x-distribution of IC quarks. Distribution (18) has its maximum at $x = 1/7$ which is close enough to the peak of distribution (4), see fig. 2.

The fragmentation functions of non-charmed quarks and diquarks into charmed mesons and baryons are taken from [10]:

$$\begin{aligned}
G_u^{\overline{D^0}} = G_d^{D^-} &= a_0(1-z)^{\lambda-\alpha_\psi(0)}(1+a_1 z^2), \\
G_u^{D^-} = G_u^{D^+} = G_u^{D^0} = G_d^{D^+} = G_d^{D^0} = G_d^{\overline{D^0}} &= a_0(1-z)^{1+\lambda-\alpha_\psi(0)}, \\
G_{uu}^{D^+} = G_{uu}^{D^-} = G_{uu}^{D^0} = G_{ud}^{D^+} = G_{ud}^{D^0} &= a_0(1-z)^{3+\lambda-\alpha_\psi(0)}, \\
G_{uu}^{\overline{D^0}} &= a_0(1-z)^{2+\lambda-\alpha_\psi(0)}(1+a_2 z^2), \\
G_{ud}^{\overline{D^0}} &= a_0(1-z)^{2+\lambda-\alpha_\psi(0)}(1-z+a_2 z^2/2), \\
G_{uu}^{\Lambda_c} = G_{ud}^{\Lambda_c} &= a_{01}(1-z)^{6+\lambda-\alpha_\psi(0)}, \\
G_u^{\Lambda_c} = G_d^{\Lambda_c} &= a_{01}(1-z)^{2+\lambda-\alpha_\psi(0)}, \\
G_{\bar{u}}^{\Lambda_c} = G_{\bar{d}}^{\Lambda_c} &= G_u^{\Lambda_c}(1-z),
\end{aligned} \tag{20}$$

with

$$\alpha_\psi(0) = -2\ ,\ \lambda = 0.5\ ,\ a_0 = 0.02\ ,\ a_{01} = 0.016\ ,\ a_1 = 20\ ,\ a_2 = 100. \tag{21}$$

As far as Λ_c production is concerned, there are two different contributions [6]. The first one corresponds to the central production of $\Lambda_c\overline{\Lambda_c}$ pairs and can be described by the formulae presented above. The second contribution is connected with the direct fragmentation of the initial baryon into Λ_c with string junction conservation. To account for this possibility we input into eq. (11) two additional terms, $f_{qq2}(x_+, n)$ and $f_{qq2}(x_-, n)$, which are not multiplied by $f_q(x_-, n)$ and $f_q(x_+, n)$. These terms are derived using the corresponding fragmentation functions:

$$\begin{aligned}
G_{uu2}^{\Lambda_c} &= a_{02} z^2(1-z)^{1+\lambda-\alpha_\psi(0)}, \\
G_{ud2}^{\Lambda_c} &= a_{02} z^2(1-z)^{\lambda-\alpha_\psi(0)},
\end{aligned} \tag{22}$$

with

$$a_{02} = 1. \tag{23}$$

The fragmentation functions of charmed quarks into D mesons and Λ_c baryon are really unknown[1)] so they are assumed to be similar to the fragmentation functions of strange quarks into K mesons and Λ_s baryon:

$$\begin{aligned}
G_{(c+\bar{c})/2}^{D^+} = G_{(c+\bar{c})/2}^{\overline{D^0}} &= G_{(c+\bar{c})/2}^{D^0} = G_{(c+\bar{c})/2}^{D^-} = \frac{1}{2} a_{c0} z(1-z)^{\lambda-\alpha_R(0)} + a_{c1}(1-z)^{2+\lambda-\alpha_R(0)}, \\
G_{(c+\bar{c})/2}^{\Lambda_c} &= a_{c2}[z(1-z)^{3+\lambda+\alpha_R(0)} + 3z(1-z)^{1+\lambda+\alpha_R(0)},
\end{aligned} \tag{24}$$

1) Notice that the fragmentation functions in QGSM differ from the fragmentation functions used in PFM hard processes.

and in the case of string junction conservation:

$$G^{\Lambda_c}_{(c+\bar{c})/2} = a_{c3} z^2 (1-z)^\lambda (1 - 0.95z + .03z^2),$$
$$a_{c0} = 0.687\ ,\ a_{c1} = 0.26\ ,\ a_{c2} = 0.15\ ,\ a_{c3} = 0.15\ . \qquad (25)$$

The probabilities of processes with n cut pomerons are also taken from [10].

4. INCLUSIVE SPECTRA OF CHARMED HADRONS IN pp COLLISIONS

Here we perform PFM calculations as in [2], including the same IC component in a proton but using a more "modern" set of proton structure functions, namely set MT (S-DIS) [12], then compare the results with analogous QGSM predictions.

Despite the fact that the IC mechanism gives a relatively small contribution to the total charm production cross-section, it can significantly modify the shape of the differential cross-sections at large x_F. In the pp center-of-mass frame, a convenient parametrization of the momenta is:

$$\begin{aligned} p_a &= \frac{\sqrt{s}}{2}(x_a, 0, x_a), \\ p_b &= \frac{\sqrt{s}}{2}(x_b, 0, -x_b), \\ p_i &= (\hat{m}_i \cosh y_i, p_{Ti}, \hat{m}_i \sinh y_i), \qquad i = 1, \dots, 4, \end{aligned} \qquad (26)$$

where p_1 and p_2 are the momenta of the produced heavy quarks and p_3 and p_4 refer to the charmed hadrons obtained after the fragmentations $1 \to 3$ and $2 \to 4$. The partons a and b are considered as massless.

Starting from the formula [2]:

$$E_3 E_4 \frac{d\sigma}{d^3p_3 d^3p_4} = \int \frac{s}{2\pi} \frac{dx_a}{x_a} \frac{dx_b}{x_b} dz_3 dz_4 H_{ab}(x_a, x_b) \frac{E_3 E_4}{E_1 E_2} \frac{D_{H/c}(z_3)}{z_3^3} \frac{D_{H/c}(z_4)}{z_4^3} \delta^4(p_a + p_b - p_1 - p_2), \qquad (27)$$

where:

$$H_{ab} = \sum_{all\ q\bar{q}} [x_a G_q(x_a)] [x_b G_{\bar{q}}(x_b)] \left. \frac{d\hat{\sigma}}{d\hat{t}} \right|_{q\bar{q}} + [x_a G_g(x_a)] [x_b G_g(x_b)] \left. \frac{d\hat{\sigma}}{d\hat{t}} \right|_{gg} .$$

the inclusive x-distribution of a single charmed hadron is equal to:

$$\frac{d\sigma_{PF}}{dx} = \frac{\sqrt{s}}{2} \int H_{ab}(x_a, x_b) \frac{1}{E_1} \frac{D_{H/c}(z_3)}{z_3} dy_2 dp_T^2 dz_3. \qquad (28)$$

Taking into account eq. (8), the total differential cross-sections of charmed hadrons with PF and IC contributions are:

$$\begin{aligned} \frac{d\sigma}{dx_D} &= \frac{2}{3} \left(\frac{d\sigma_{PF}}{dx_D} + \sigma_{IC} \frac{dN}{dx_D} \right), \\ \frac{d\sigma}{dx_{\overline{D}}} &= \frac{d\sigma_{PF}}{dx_{\overline{D}}} + \sigma_{IC} \frac{dN}{dx_{\overline{D}}}, \\ \frac{d\sigma}{dx_{\Lambda_c}} &= \frac{1}{3} \left(\frac{d\sigma_{PF}}{dx_{\Lambda_c}} + \sigma_{IC} \frac{dN}{dx_{\Lambda_c}} \right), \end{aligned} \qquad (29)$$

where dN/dx stands for each $d\sigma_{IC}/dx$ distribution normalized to unity.

So far (eqs. (29)) the shapes of the D, $\overline{D}$ and Λ_c distributions are predicted to be the same since the fragmentation function (eq. (5) in eqs. (7) and (28)) is the same. However $\overline{D}$ mesons as well as Λ_c baryons can be produced [2] via recombination of $\bar{c}$ or c quarks with u or d valence quarks. In [2] it was assumed that such recombination mechanism is possible only for intrinsic charm quarks and the corresponding cross-sections take the form:

$$\left(\frac{d\sigma_{IC}}{dx_{\Lambda_c}}\right)_R = \int \frac{d\sigma_{IC}}{dx_1 dx_2 dx_3 dx_c dx_{\bar{c}}} \delta(x_{\Lambda_c} - x_1 - x_2 - x_c)\, dx_1 dx_2 dx_3 dx_c dx_{\bar{c}} \qquad (30)$$

and

$$\left(\frac{d\sigma_{IC}}{dx_{\overline{D}}}\right)_R = \int \frac{d\sigma_{IC}}{dx_1 dx_2 dx_3 dx_c dx_{\bar{c}}} \delta(x_{\overline{D}} - x_1 - x_{\bar{c}}) dx_1 dx_2 dx_3 dx_c dx_{\bar{c}}. \qquad (31)$$

The distributions (30) and (31), normalized to unity, are presented in fig. 3. With 50% of intrinsic charm recombination for $\overline{D}$ and Λ_c production, eqs. (29) become:

$$\begin{aligned}
\frac{d\sigma}{dx_D} &= \frac{2}{3}\left[\frac{d\sigma_{PF}}{dx_D} + \sigma_{IC}\frac{dN}{dx_D}\right], \\
\frac{d\sigma}{dx_{\overline{D}}} &= \frac{d\sigma_{PF}}{dx_{\overline{D}}} + \sigma_{IC}\left(\frac{1}{2}\frac{dN}{dx_{\overline{D}}} + \frac{1}{2}\frac{dN_R}{dx_{\overline{D}}}\right), \\
\frac{d\sigma}{dx_{\Lambda_c}} &= \frac{1}{3}\left[\frac{d\sigma_{PF}}{dx_{\Lambda_c}} + \sigma_{IC}\left(\frac{1}{2}\frac{dN}{dx_{\Lambda_c}} + \frac{1}{2}\frac{dN_R}{dx_{\Lambda_c}}\right)\right],
\end{aligned} \qquad (32)$$

where dN/dx stands for each $d\sigma_{IC}/dx$ distribution due to fragmentation (as in eqs. (29)) and dN_R/dx for each $(d\sigma_{IC}/dx)_R$ distribution due to recombination, normalized to unity.

In fig. 4 and fig. 5 the experimental x_F-distributions for D and $\overline{D}$ production at $p_{lab} = 400$ GeV/c [13] and for Λ_c at $\sqrt{s} = 62$ GeV [17] are presented together with the results of our calculations. The predictions of PFM with IC contribution, given by eqs. (32), are shown as thin solid curves for Peterson fragmentation function and as dashed curves for $\delta(z-1)$ fragmentation function. The calculations were performed at the QCD leading order (LO $\sim \alpha_s^2$) and next-to-leading order (NLO) contributions were accounted for via multiplying the LO results by the K-factors calculated in [16]. We can see that eqs. (32) give some better description of $\overline{D}$ meson production (with respect to D meson). However, in the case of Λ_c production, they predict a shoulder in the distributions at large x_F which is still two orders of magnitude below the experimental data. These results are in agreement with [2].

Thick solid curves in figs. 4 and 5 show the predictions of QGSM with the same IC contribution as in PFM. Contrary to the PFM case, here the best agreement is found for Λ_c, whose "leading effect" is reasonably reproduced. Let us briefly recall that the so-called "leading effect" [18, 19] is related to the number of valence quarks propagating from the initial to the final state: two for Λ_c, one for $\overline{D}$ and zero for D in pp collisions. The effect corresponds to an abundant Λ_c production in the high x_F-region, therefore to a Λ_c distribution $d\sigma/dx_F \propto (1-x_F)^{\sim 2}$, as measured in pp at $\sqrt{s} = 62$ GeV [17, 20], see fig. 5. Indeed this distribution differs from the corresponding $\overline{D}$ [13] and D [13, 21] distributions, also measured in pp at the same or lower energy, see fig. 4. Notice that previous QGSM calculations without intrinsic charm [10] produced similar results using harder diquark fragmentation functions (eqs. (22) with $a_{02} = 2$). In addition it should be stressed that in QGSM we do not need the same recombination formalism as in PFM, the reason being that the fragmentation functions used are actually different for sea and valence quarks (and diquarks), see sect. 3.

5. INTRINSIC CHARM CONTRIBUTION TO PHOTOPRODUCTION IN PFM

In heavy flavour photoproduction the main contribution is given by γg fusion, but by resolving a photon also gg as well as $q\overline{q}$ fusion can be taken in account (fig. 6). Usually the last two contributions give no more than $20 \div 30\%$ of the total cross-section for charm production. However at very high energies ($\sqrt{s} > 500$ GeV) these two contributions increase, which may be partly due to our lack of knowledge of the photon structure functions in the very small x-region. As an example, in table 2 we give the partial cross-sections relative to γg, gg and $q\overline{q}$ subprocesses at different energies, as obtained using MT (S-DIS) structure functions for the proton and GRV-G (HO) for the resolved photon [22].

In the case of γp interactions there are much less experimental data available as inputs for our calculations. An estimate of the amount of intrinsic charm released in γp interactions can be obtained in the spirit of [2] assuming the following relations:

$$w_{IC} = \frac{1}{2}\left(\frac{\sigma_{IC}}{\sigma_{inel}}\right)_{pp} \approx \left(\frac{\sigma_{IC}}{\sigma_{inel}}\right)_{\gamma p} \approx 10^{-5}, \qquad \sigma_{IC}(\gamma p) \approx 1\ nb. \tag{33}$$

The IC production probability w_{IC} is very small but it cannot be significantly increased without contradicting the experimental data on D and $\overline{D}$ production in pp interactions (see fig. 4). This probability is a product of two factors:

$$w_{IC} = \beta^2 \cdot \eta, \tag{34}$$

where β^2 is the probability to find a $c\overline{c}$ pair and η is the probability that this pair will fragment into charmed hadrons in the soft interaction process. The experimental estimate of β^2 from μp interaction data [23] is about 0.003 and a somewhat higher value $\beta^2 = 1\%$ was used in [24] for IC calculations in DIS processes. Of course, if the charm quark inside the proton absorbs a γ^* at large Q^2, it will fragment into a charmed hadron with $\sim$ 100% probability, so $\eta \approx 1$. However in the case of soft collisions, there is an additional suppression factor [25], coming from the need to resolve the IC state since IC quarks are at small distances with respect to each other, so the value of η should be relatively small. We can try to give the simplest estimate of η for soft interactions. The probability for light valence quark transition into π or K meson (not into baryon) in soft pp collisions can be estimated from the difference between π^+ and π^-, or K and $\overline{K}$, multiplicities at intermediate x_F-values. This probability is about $0.2 \div 0.3$ and it should be multiplied by the squared ratio of the distance between c and $\overline{c}$ over the proton diameter. This factor is roughly $(m_q/m_c)^2 \sim 1/25$ if we use the constituent quark masses. So we obtain $\eta \sim 10^{-2}$ and (from eqs. (33) and (34)) $\beta^2 \sim 0.003$ which does not contradict the experimental data. Of course, a smaller value of β^2 is also possible.

The σ_{IC} value (33) is very small as compared with the values of table 2. Nevertheless we know that the IC component can change the shape of the charmed hadron distributions and we will study its effects in more details.

Figure 7 shows the contributions of PF and IC processes as seen in the γp centre-of-mass frame when the x_F-distribution of D mesons is considered at different energies. The γ direction is chosen to be the positive axis. To compute the processes presented in fig. 6 we use the formulae [2, 26]:

$$
\begin{aligned}
\frac{d\hat{\sigma}^{\gamma g\to c\bar{c}}}{d\hat{t}} &= \frac{\pi}{\hat{s}^2}\alpha_s\alpha_{em}e_c^2\frac{\hat{u}^2+\hat{t}^2}{\hat{u}\hat{t}}, \\
\frac{d\hat{\sigma}^{gg\to c\bar{c}}}{d\hat{t}} &= \frac{\pi\alpha_s^2}{96\hat{m}_c^4}\frac{8\cosh(y_1-y_2)-1}{(1+\cosh(y_1-y_2))^3}\left(\cosh(y_1-y_2)+\frac{2m_c^2}{\hat{m}_c^2}-\frac{2m_c^4}{\hat{m}_c^4}\right), \\
\frac{d\hat{\sigma}^{q\bar{q}\to c\bar{c}}}{d\hat{t}} &= \frac{\pi\alpha_s^2}{9\hat{m}_c^4}\frac{\cosh(y_1-y_2)+\frac{m_c^2}{\hat{m}_c^2}}{(1+\cosh(y_1-y_2))^3},
\end{aligned}
\tag{35}
$$

where y_1 and y_2 are the rapidities of the produced c and $\bar{c}$-quarks and e_c their electric charge.

The calculations have been performed using Peterson fragmentation function and the IC contribution does not seem to affect the shape of the differential D meson cross-section in fig. 7. However, by including the recombination mechanism, some modifications occur. For example, if we assume that one half of all IC quarks hadronize via recombination with valence quarks, we obtain a "shoulder" in the spectra of $\overline{D}$ and Λ_c at $x_F < -0.5$ as one can see in figs. 8 and 9. Notice that the shapes of all curves in figs. 7-9 depend significantly on the fragmentation function used.

The results obtained so far with Peterson fragmentation plus recombination can be compared with Monte Carlo predictions for D and $\overline{D}$ production. To this purpose we use PYTHIA 5.6 [27] (where there is no intrinsic charm component) with all default parameters but a second order expression for α_s. In fig. 10 one can see a general qualitative agreement of the Monte Carlo with our IC calculations in particular at high energies. But there is also a systematic difference. In PYTHIA the difference between the D and $\overline{D}$ spectra is significantly smaller in the negative x_F-region than in our calculations with 50% probability of intrinsic charm recombination. At large positive x_F-values, PYTHIA predicts higher cross-sections for D and $\overline{D}$ production.

Let us now consider the Feynman-x distribution of $c\bar{c}$ pairs produced in γp collisions. Intrinsic $c\bar{c}$ pairs should have a larger average x than single charm quarks. Therefore their IC effects should be more visible. Moreover the main γg fusion subprocess in PFM gives no contribution to pair production in the incident proton direction (i.e. at negative x_F).

The γg contribution to the charm photoproduction cross-section is [28]:

$$
\frac{d\sigma^{\gamma p\to c\bar{c}}}{dx_g} = G(x_g, Q^2)\hat{\sigma}^{\gamma g\to c\bar{c}}(x_g s, m_c, Q^2), \tag{36}
$$

where $G(x_g, Q^2)$ is the gluon structure function of the proton, with $x_g \geq 4m_c^2/s$. Longitudinal momentum conservation gives:

$$
1 - x_g = x_c + x_{\bar{c}} \tag{37}
$$

and from eq. (36), with the change of variable $x_{pair} = 1 - x_g$, the differential cross-section of $c\bar{c}$ pairs is easily obtained:

$$\frac{d\sigma}{dx_{pair}} = \left[G(x_g, Q^2)\hat{\sigma}(x_g s, m_c, Q^2)\right]_{x_g=1-x_{pair}}, \tag{38}$$

with $x_{pair} \leq 1 - 4m_c^2/s$.

The pair cross-section at large x_{pair} is given by small x_g, where the gluon structure function is large. There is no second structure function as in eq. (3) for suppression.

Similarly, for gg and $q\bar{q}$ fusion, the changes of variables:

$$\begin{cases} x_+ = x_a + x_b \\ x_- = x_a - x_b \end{cases} \tag{39}$$

transform expression (3) into:

$$\sigma^{\gamma p\to c\bar{c}} = \int_{x_-^{min}}^{x_-^{max}} dx_- \int_{x_+^{min}}^{x_+^{max}} dx_+ \, \frac{1}{2}\frac{x_a G(x_a)}{x_a}\frac{x_b G(x_b)}{x_b}\hat{\sigma}^{ab\to c\bar{c}}(x_a x_b s, m_c^2, Q^2), \tag{40}$$

with the notations:

$$\begin{aligned} x_-^{min} &= \frac{4m_c^2}{s} - 1, \\ x_-^{max} &= 1 - \frac{4m_c^2}{s}, \\ x_+^{min} &= \sqrt{\frac{16m_c^2}{s} + x_-^2}, \\ x_+^{max} &= 2 - |x_-|. \end{aligned}$$

The variable $x_- = x_a - x_b$ is the fractional momentum of the $c\bar{c}$ pair due to momentum conservation:

$$x_a - x_b = x_c + x_{\bar{c}}. \tag{41}$$

Denoting $\prod dx_i$ the product $dx_1 dx_2 dx_3 dx_c dx_{\bar{c}}$, the intrinsic distribution of the $c\bar{c}$ pair is given by:

$$\frac{d\sigma_{IC}}{dx_{pair}} = \int \prod dx_i \, \frac{d\sigma_{IC}}{\prod dx_i}\,\delta(x_{pair} - x_c - x_{\bar{c}}). \tag{42}$$

The x-distribution of $D\bar{D}$ pairs from IC fragmentation is the result of the convolution:

$$\frac{dN}{dx_{pair}} = \int \prod dx_i dz_D dz_{\bar{D}} \frac{d\sigma_{IC}}{\prod dx_i} D_{D/c}(z_D) D_{\bar{D}/\bar{c}}(z_{\bar{D}})\delta(x_{pair} - z_D x_c - z_{\bar{D}} x_{\bar{c}}). \tag{43}$$

Figure 11 shows the difference in shape between the $c\bar{c}$ and $D\bar{D}$ distributions of eqs. (42) and (43), normalized to unity, with Peterson fragmentation function.

The x_F-distributions of $c\bar{c}$ pairs produced in γp interactions at different energies are shown in fig. 12 (PF only) and in fig. 13 (PF plus IC). The same results hold true for $D\bar{D}$ production once δ-function fragmentation is assumed for charm quarks. At low energy ($\sqrt{s}$ = 10 GeV) one can see a kinematical limit in the spectra of figs 12a and 13a at $(x_F)_{pair} \approx 0.9$ which is connected with our definition of $(x_F)_{pair}$ as $2(p_L)_{pair}/\sqrt{s}$ and not as $(p_L)_{pair}/(p_{Lmax})_{pair}$, where $(p_L)_{pair}$ and $(p_{Lmax})_{pair}$ are the total longitudinal momentum of the pair and its maximum possible value at a given energy, respectively. Intrinsic charm pairs make the spectrum flatter at negative x_F (i.e. in the proton direction) and this effect is more important at low energy. As already seen in pp (fig. 4), δ-function fragmentation gives a slightly better agreement with the experimental data. So we may retain it, especially keeping in mind the possibility of charm recombination with valence quarks.

6. CONCLUSIONS

In the Parton Fusion Model (PFM) description of pp collisions, the intrinsic charm (IC) mechanism can substantially modify the inclusive spectra of charmed hadrons, as discussed in [2]. In fact, the PFM predictions presented herein seem to agree better with the experimental x_F-distributions of D mesons (especially $\overline{D}$) at $\sqrt{s}$ = 27 GeV if an adequate IC component is included, in accordance with [2]. However PFM, with the same IC contribution, is unable to reproduce the Λ_c baryon spectrum measured at $\sqrt{s}$ = 62 GeV, although this contribution shows up at large x_F. Notice that our PFM results are obtained in the K·LO approximation (where LO results are multiplied by appropriate K-factors to account for NLO contributions) and we know that LO+NLO calculations may produce different inclusive spectra for charmed hadrons, even if the total cross-sections are the same.

On the other hand, as shown in [10], the Quark-Gluon String Model (QGSM) can reasonably describe both the D meson and Λ_c baryon experimental x_F-distributions without invoking any intrinsic charm. The introduction of an IC contribution in QGSM (of the same entity as in PFM) does not significantly change the results.

Also in γp interactions the IC mechanism may influence the longitudinal distributions of charmed hadrons obtained with PFM, as it appears from our detailed study of D, $\overline{D}$ and Λ_c production at different energies. However in this case our predictions critically depend on a given number of assumptions, or "reasonable guesses", which are not based on experimental inputs as in the pp case.

Nevertheless, what should be pointed out is that, either in pp or γp interactions, IC effects are enhanced when the recombination of intrinsic quarks with valence quarks inside the proton is allowed, since it leads to a broader x-distribution for the produced charm hadrons. In particular, in γp processes, Peterson fragmentation without recombination decreases too much the average x for an IC effect to be visible. But, let us stress it again, even with recombination the IC mechanism in PFM cannot predict the "leading baryon" behaviour of Λ_c: this has been experimentally observed in pp interactions and it is expected to appear also in γp interactions, in the incident proton direction.

Finally, in γp processes at high energies (which are of course interesting for HERA experiments), the parton structure of the photon becomes relevant for charm production and should be studied in more details. This can be done with $c\bar{c}$ pairs, rather than single charm, whose production should be more sensitive to the various resolved photon contributions, in particular as far as IC effects are concerned.

ACKNOWLEDGEMENTS

We are grateful to S. J. Brodsky, Yu. Dokshitzer, G. Ingelman, V. A. Khoze and R. Vogt for interesting discussions.

Table 1

Total cross-section for charm production in pp collisions at different energies. The predictions of the Parton Fusion Model are compared with the corresponding experimental data [13, 14].

p_{lab} (GeV/c)	200	400	800
$\sqrt{s}$ (GeV)	19.4	27.4	38.8
$\sigma_{PF}^{pp\to c\bar{c}}$ (μb)	5	13.5	29
$\sigma_{exp}^{pp\to c\bar{c}}$ (μb)	-	$14 \div 23$ [13]	$29 \div 55$ [14]

Table 2

The contributions from the Parton Fusion Model diagrams of fig. 6 to the total cross-section for charm production in γp interactions at different energies.

$\sqrt{s}$ (GeV)	$\sigma(\gamma g \to c\bar{c})$ (μb)	$\sigma(gg \to c\bar{c})$ (μb)	$\sigma(q\bar{q} \to c\bar{c})$ (μb)
10	0.19	0.0006	0.0024
50	1.07	0.080	0.012
100	1.33	0.22	0.017
300	1.85	0.69	0.029
500	2.20	1.08	0.039

FIGURE CAPTIONS

Fig. 1 : QGSM diagrams representing to the one-pomeron exchange contribution to the elastic pp scattering (cylindrical diagram) (a) and the contribution to the inelastic pp cross-section determined by the cut of one pomeron (b) and of three pomerons (c).

Fig. 2 : x-distributions (normalized to unity) for intrinsic $c(\bar{c})$ quarks (dashed curve) and $D(\overline{D})$ (or $\Lambda_c(\overline{\Lambda_c})$) hadrons after Peterson fragmentation (solid curve).

Fig. 3 : x-distributions (normalized to unity) for $\overline{D}$ mesons (a) and Λ_c baryons (b) after recombination of intrinsic $c(\bar{c})$-quarks with valence quarks in the proton.

Fig. 4 : The x_F-distributions of D mesons (a) and $\overline{D}$ mesons (b) measured in pp collisions at $\sqrt{s} = 27$ GeV [13]. The PFM+IC predictions are shown as thin solid curves for Peterson fragmentation and as dashed curves for δ-function fragmentation. In the case of $\overline{D}$ mesons, the curves are obtained assuming that IC quarks produce 50% of the $\overline{D}$'s via fragmentation and 50% via recombination with valence quarks. Thick solid curves show the QGSM predictions with the same IC contribution. The distributions refer to the $x_F > 0$ hemisphere in the pp c.m.s.

Fig. 5 : Same as fig. 4 for Λ_c baryons measured in pp collisions at $\sqrt{s} = 62$ GeV [17]. As for $\overline{D}$'s, we assume that IC quarks produce 50% of the Λ_c's via fragmentation and 50% via recombination with valence quarks. The distributions refer to the $x_F > 0$ hemisphere in the pp c.m.s.

Fig. 6 : Leading order (a) and next-to-leading order (b, c) QCD diagrams for charm photoproduction, showing the various resolved photon contributions.

Fig. 7 : PFM+IC predictions for the x_F-distribution of D mesons produced in γp interactions at different energies: $\sqrt{s} = 10$ GeV (a), 50 GeV (b), 100 GeV (c) and 300 GeV (d). Peterson fragmentation is assumed. The curves refer to the γp c.m.s. (where the direction of the incident γ is chosen to be the positive axis) and show the various contributions from γg fusion (thin solid curves), gg fusion (dashed curves), $q\bar{q}$ fusion (dash-dotted curves) and IC mechanism (dotted curves). The sum of all contributions (thick solid curves) is also shown.

Fig. 8 : Same as fig. 7 for $\overline{D}$ mesons, assuming that IC quarks produce 50% of the $\overline{D}$'s via fragmentation and 50% via recombination with valence quarks.

Fig. 9 : Same as fig. 7 for Λ_c baryons, assuming that IC quarks produce 50% of the Λ_c's via fragmentation and 50% via recombination with valence quarks.

Fig. 10 : Showing the PFM+IC predictions (thick solid curves) of fig. 7 for D mesons (a, c, e, g) and of fig. 8 for $\overline{D}$ mesons (b, d, f, h), together with the Monte Carlo predictions of PYTHIA where no IC component is included (solid points), in γp interactions at $\sqrt{s} = 10$ GeV (a, b), 50 GeV (c, d), 100 GeV (e, f) and 300 GeV (g, h).

Fig. 11 : x-distributions (normalized to unity) for intrinsic $c\bar{c}$ pairs (dashed curve) and $D\overline{D}$ pairs after Peterson fragmentation (solid curve).

Fig. 12 : PFM predictions for the x_F-distribution of $D\overline{D}$ pairs produced in γp interactions at different energies: $\sqrt{s}$ = 10 GeV (a), 50 GeV (b), 100 GeV (c) and 300 GeV (d). Delta-function fragmentation is assumed. The curves refer to the γp c.m.s. (where the direction of the incident γ is chosen to be the positive axis) and show the various contributions from γg fusion (thin solid curves), gg fusion (dashed curves) and $q\bar{q}$ fusion (dash-dotted curves). The sum of all contributions (thick solid curves) is also shown.

Fig. 13 : PFM+IC predictions for the x_F-distribution of $D\overline{D}$ pairs produced in γp interactions at different energies: $\sqrt{s}$ = 10 GeV (a), 50 GeV (b), 100 GeV (c) and 300 GeV (d). Delta-function fragmentation is assumed. The curves show the total PFM contribution (thin solid curves) taken from fig. 12, together with the contribution from IC mechanism (dotted curves). The sum of all contributions (thick solid curves) is also shown.

REFERENCES

[1] S. Banerjee and S. N. Ganguli, Phys. Rev. **D33** (1986) 1278.

[2] R. Vogt, S. J. Brodsky and P. Hoyer, Nucl. Phys. **B383** (1992) 643.

[3] R. Vogt, S. J. Brodsky and P. Hoyer, Nucl. Phys. **B360** (1991) 67.

[4] S. J. Brodsky, preprint SLAC-PUB-5529 (1991).

[5] S. J. Brodsky, P. Hoyer, A. H. Mueller and W.-K. Tang, Nucl. Phys. **B369** (1992) 519.

[6] A. B. Kaidalov and K. A. Ter-Martirosyan, Yad. Fiz. **39** (1984) 1545; **40** (1984) 211.

[7] V. A. Abramovski, V. N. Gribov and O. V. Kancheli, Yad. Fiz. **18** (1973) 595.

[8] A. B. Kaidalov and O. I. Piskunova, Yad. Fiz. **43** (1986) 1545.

[9] O. I. Piskunova, preprint FIAN-118, Moscow (1990).

[10] L. Cifarelli, E. Eskut and Yu. M. Shabelski, Nuovo Cimento **106A** (1993) 389.

[11] P. Nason, S. Dawson and R. K. Ellis, Nucl. Phys. **B303** (1988) 607.

[12] J. G. Morfin and W.-K. Tung, Z. Phys. **C53** (1991) 13.

[13] M. Aguilar-Benitez et al., Z. Phys. **C40** (1988) 321.

[14] R. Ammar et al., Phys. Lett. **B183** (1987) 110.

[15] C. Peterson, D. Schlatter, I. Schmitt and P. Zerwas, Phys. Rev. **D27**, (1983) 105.

[16] G. Anzivino et al., preprint EMCSC/93-07 (1993).

[17] G. Bari et al., Nuovo Cimento **104A** (1991) 571; M. Basile et al., Nuovo Cimento Lett. **30** (1981) 487.

[18] M. Basile et al., Nuovo Cimento **66A** (1981) 129.

[19] M. Basile et al., Nuovo Cimento Lett. **32** (1981) 321.

[20] P. Chauvat et al., Phys. Lett. **B199** (1987) 304.

[21] M. Basile et al., Nuovo Cimento Lett. **33** (1982) 33.

[22] H. Plothow-Besch, preprint CERN-PPE/92-123 (1992).

[23] E. Hoffmann and R. Moore, Z. Phys. **C20** (1983) 71.

[24] G. Ingelman, L. Jönsson and M. Nyberg, preprint DESY 92-178 (1982).

[25] S. J. Brodsky, J. C. Collins, S. D. Ellis, J. F. Gunion and A. H. Mueller, preprint DOE/ER/40048-21 (1984).

[26] R. K. Ellis, Lectures give at the 17th SLAC Summer Institute, July 1989, FERMILAB-CONF-89/168-T (1989).

[27] T. Sjöstrand, Comp. Phys. Comm. **39** (1986) 347; T. Sjöstrand and M. Bengtsson, Comp. Phys. Comm. **43** (1987) 367; H. U. Bengtsson and T. Sjöstrand, Comp. Phys. Comm. **46** (1987) 43; T. Sjöstrand and M. van Zijl, Phys. Rev. **D36** (1987) 2019; T. Sjöstrand, preprint CERN-TH.6488/92, May 1992.

[28] H. Fritzsch and K.-H. Streng, Phys. Lett. **72B** (1978) 385.

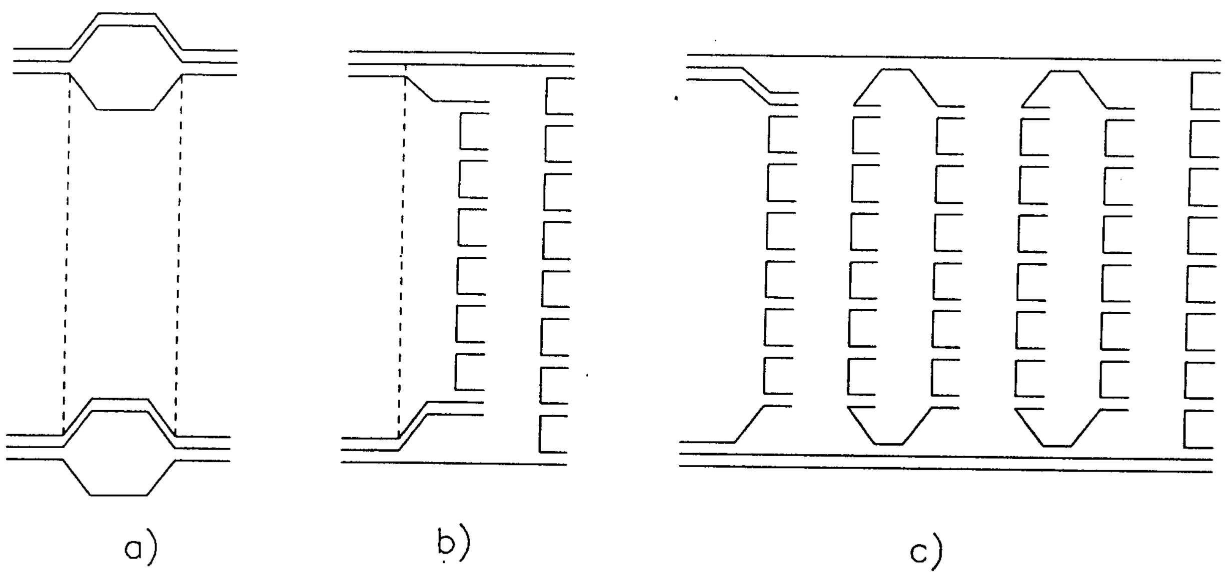

Fig. 1

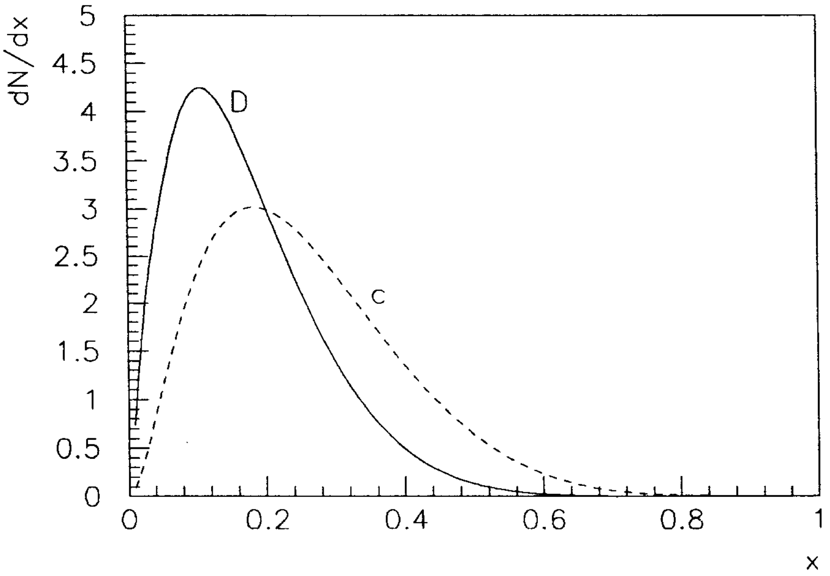

Fig. 2

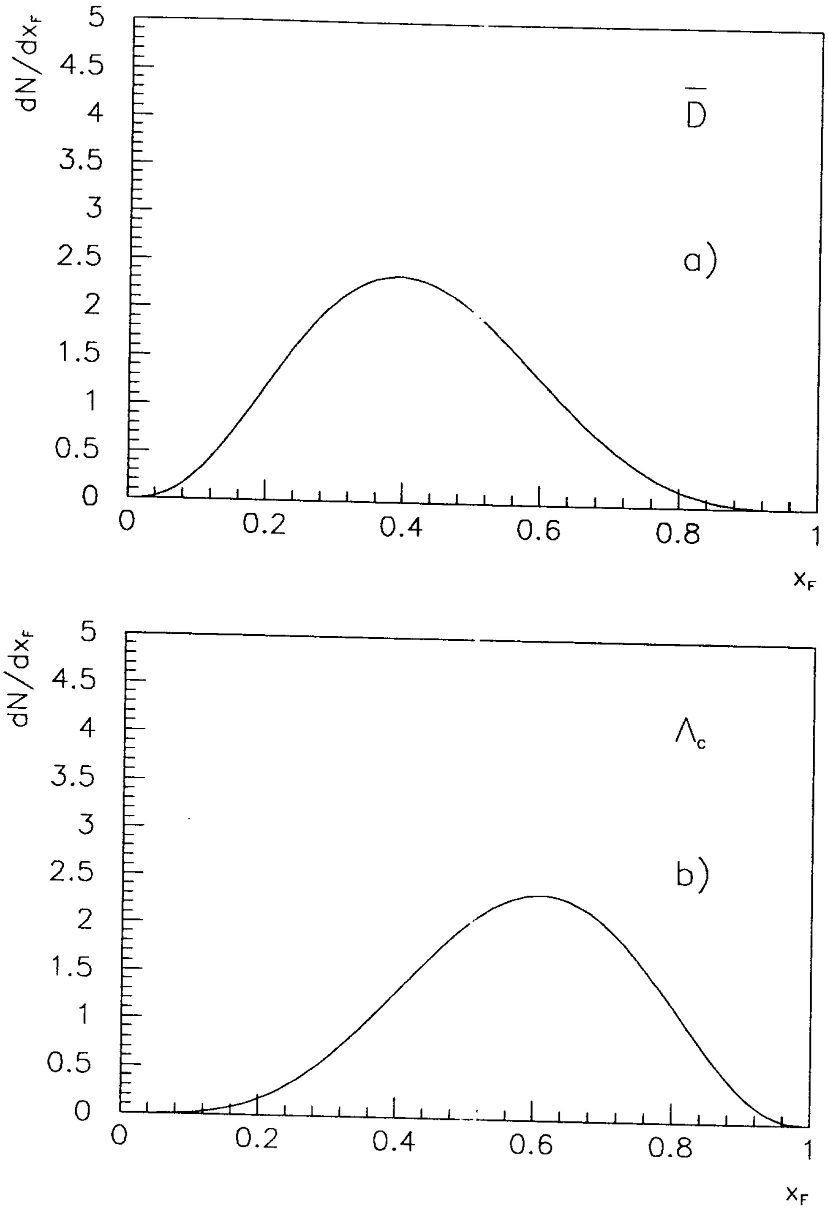

Fig. 3

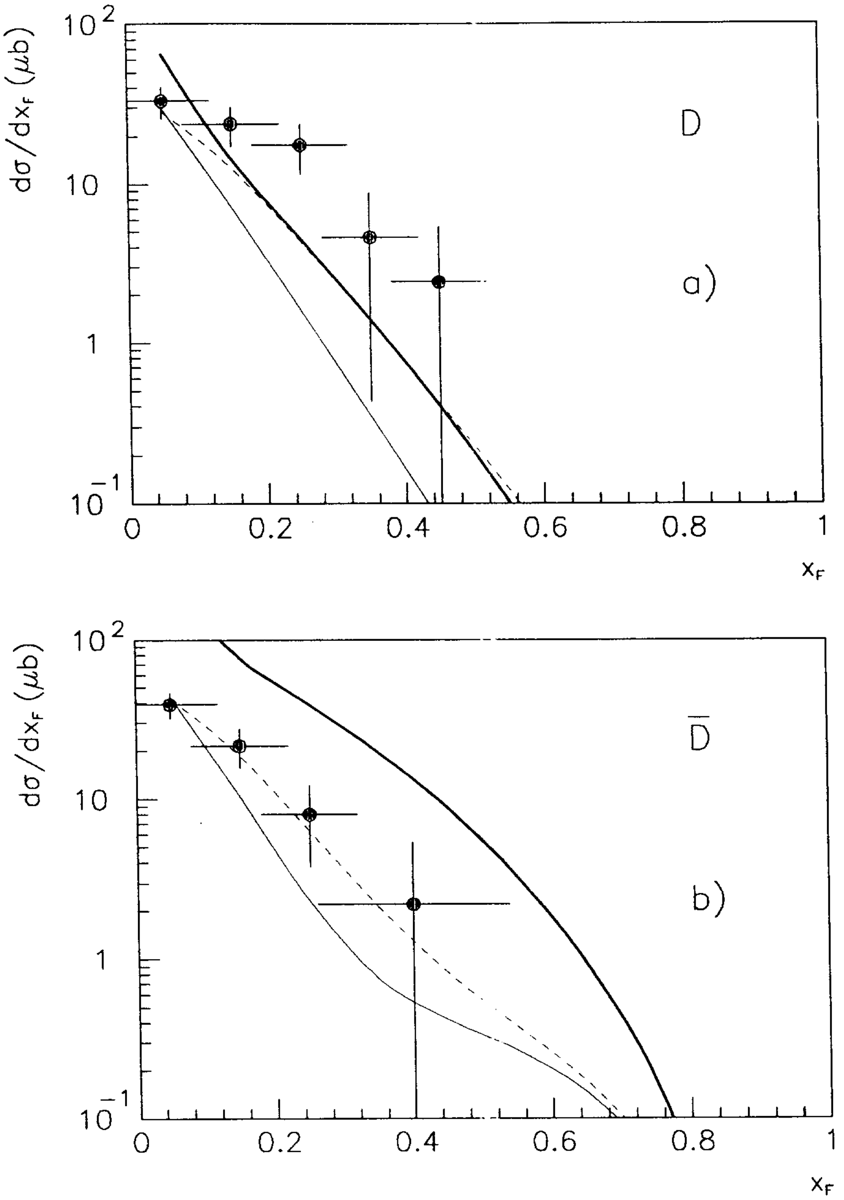

Fig. 4

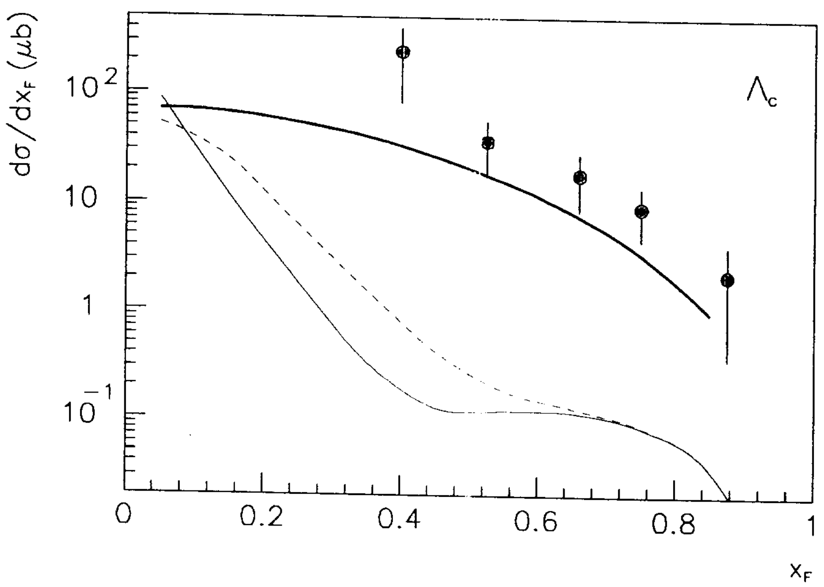

Fig. 5

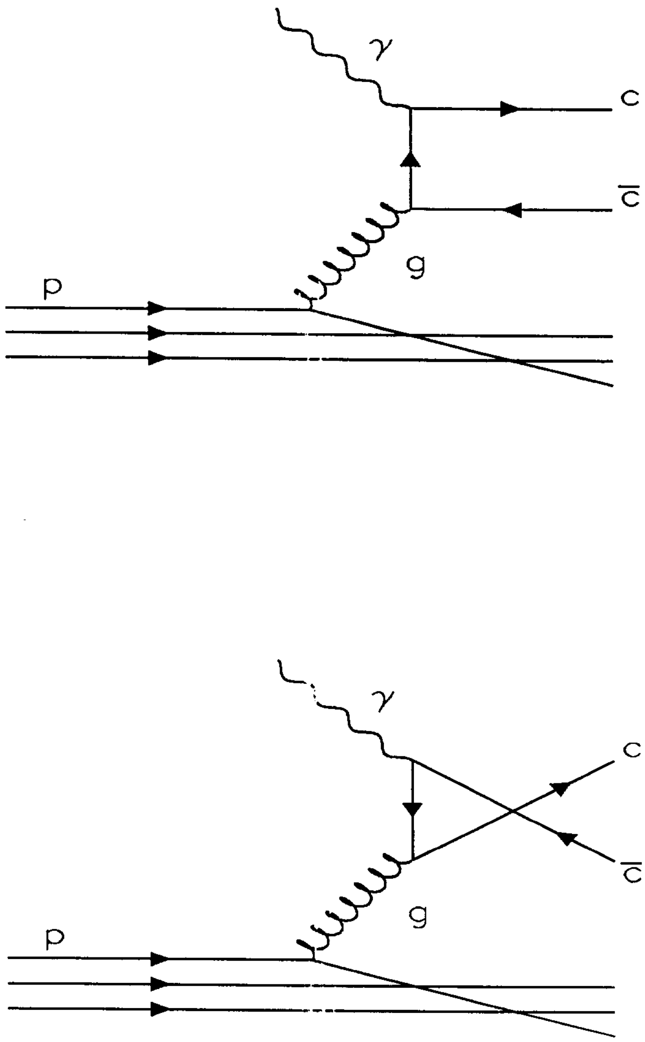

Fig. 6a

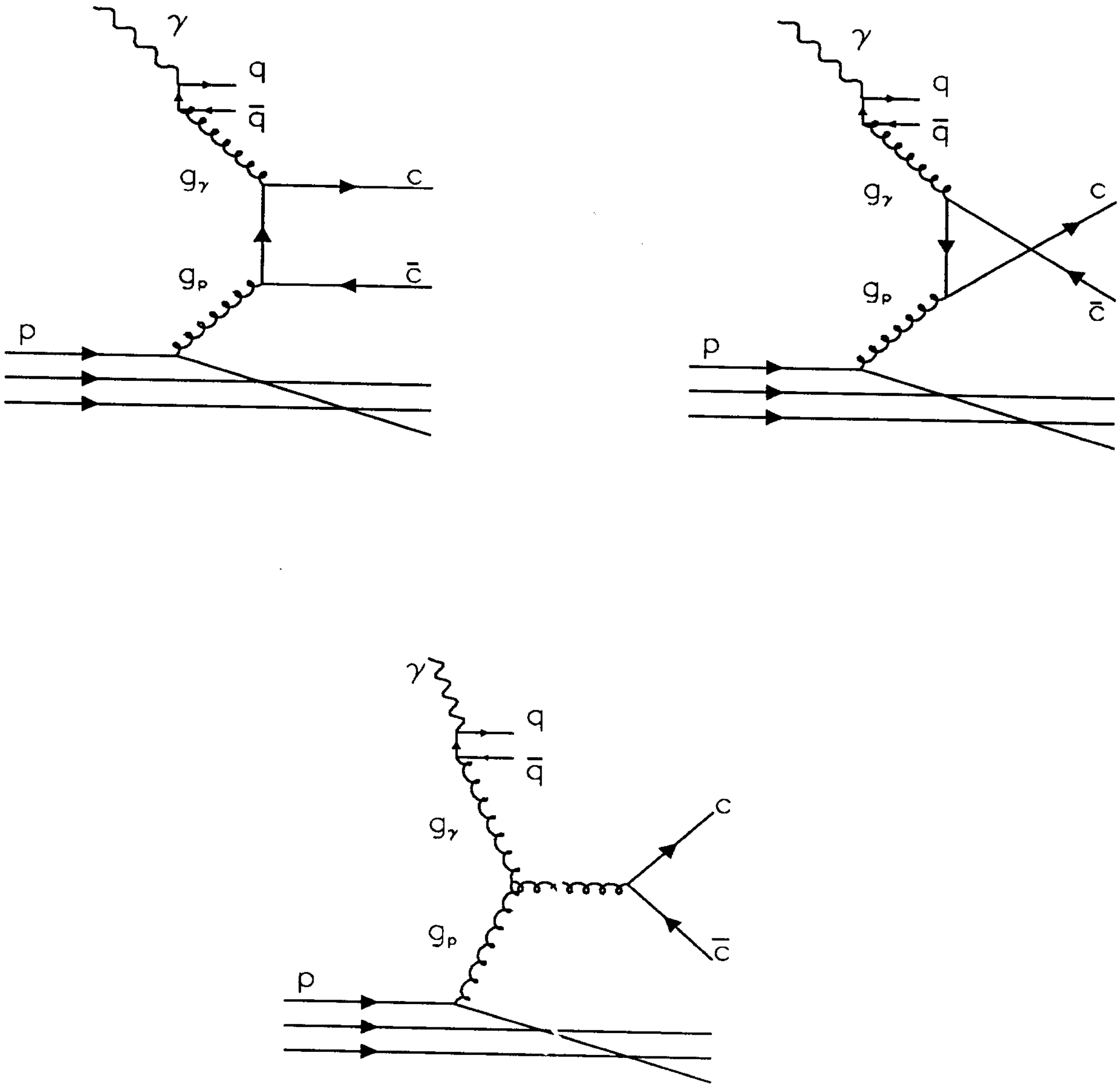

Fig. 6b

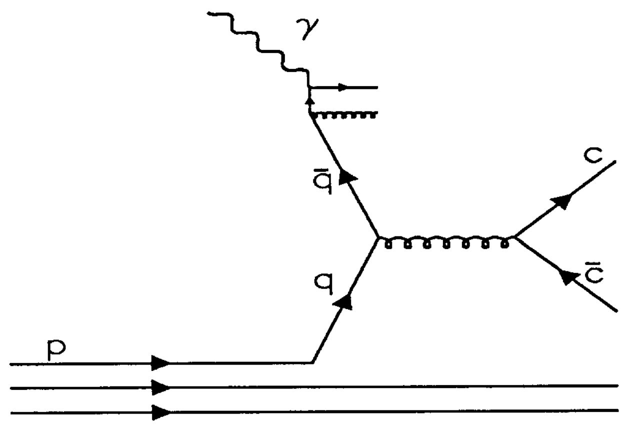

Fig. 6c

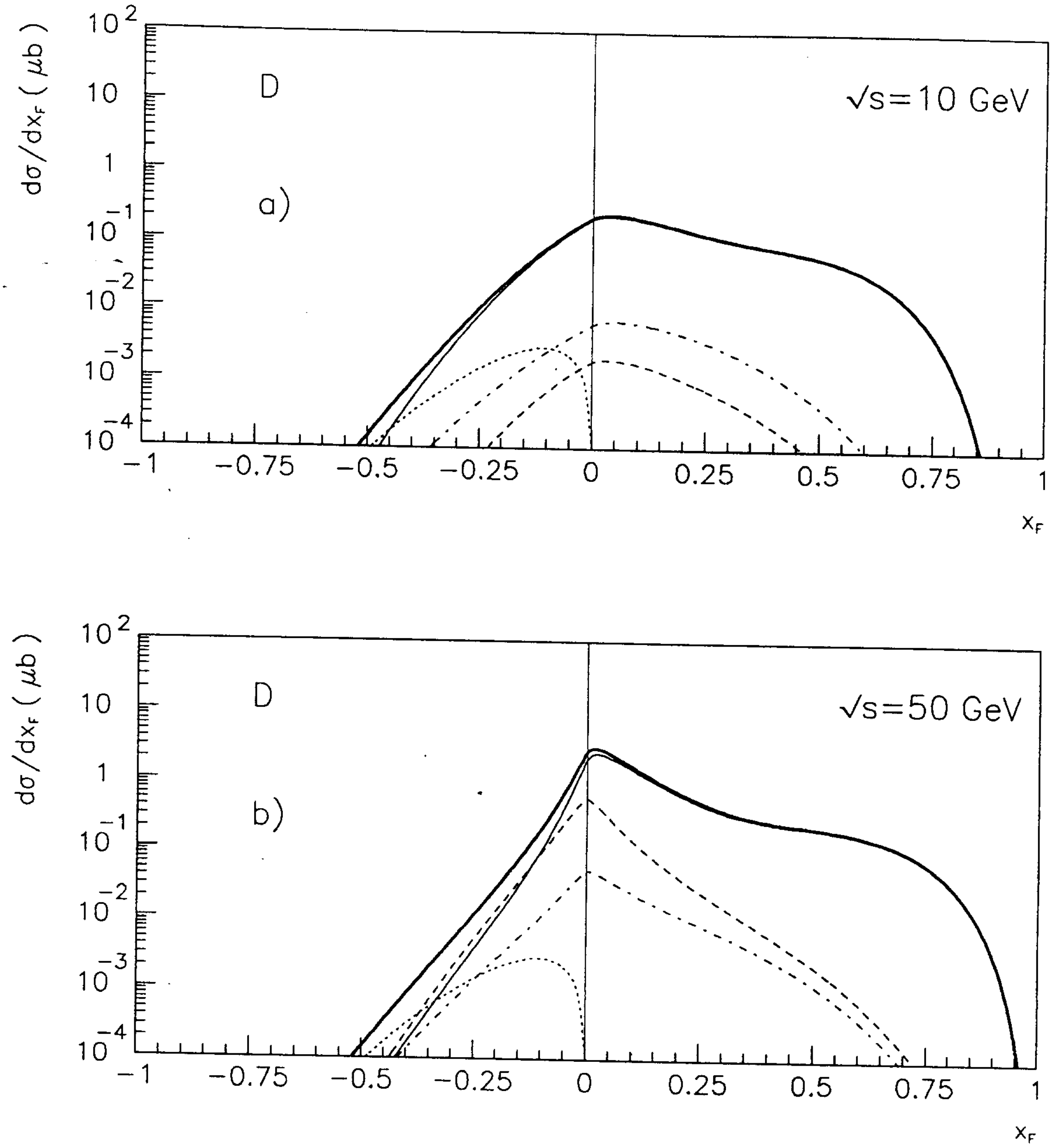

$\rightarrow \gamma$

Fig. 7a, b

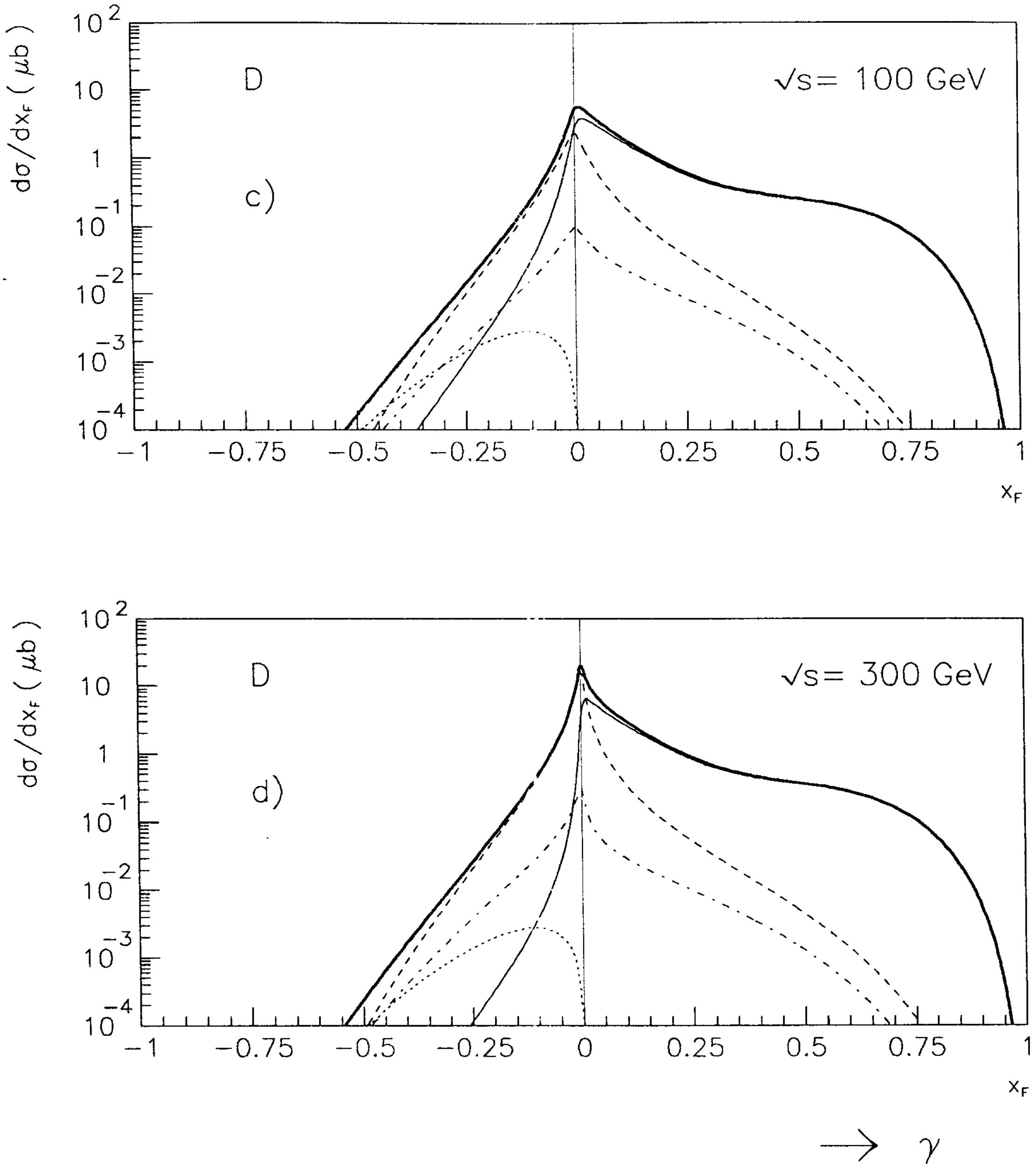

Fig. 7c, d

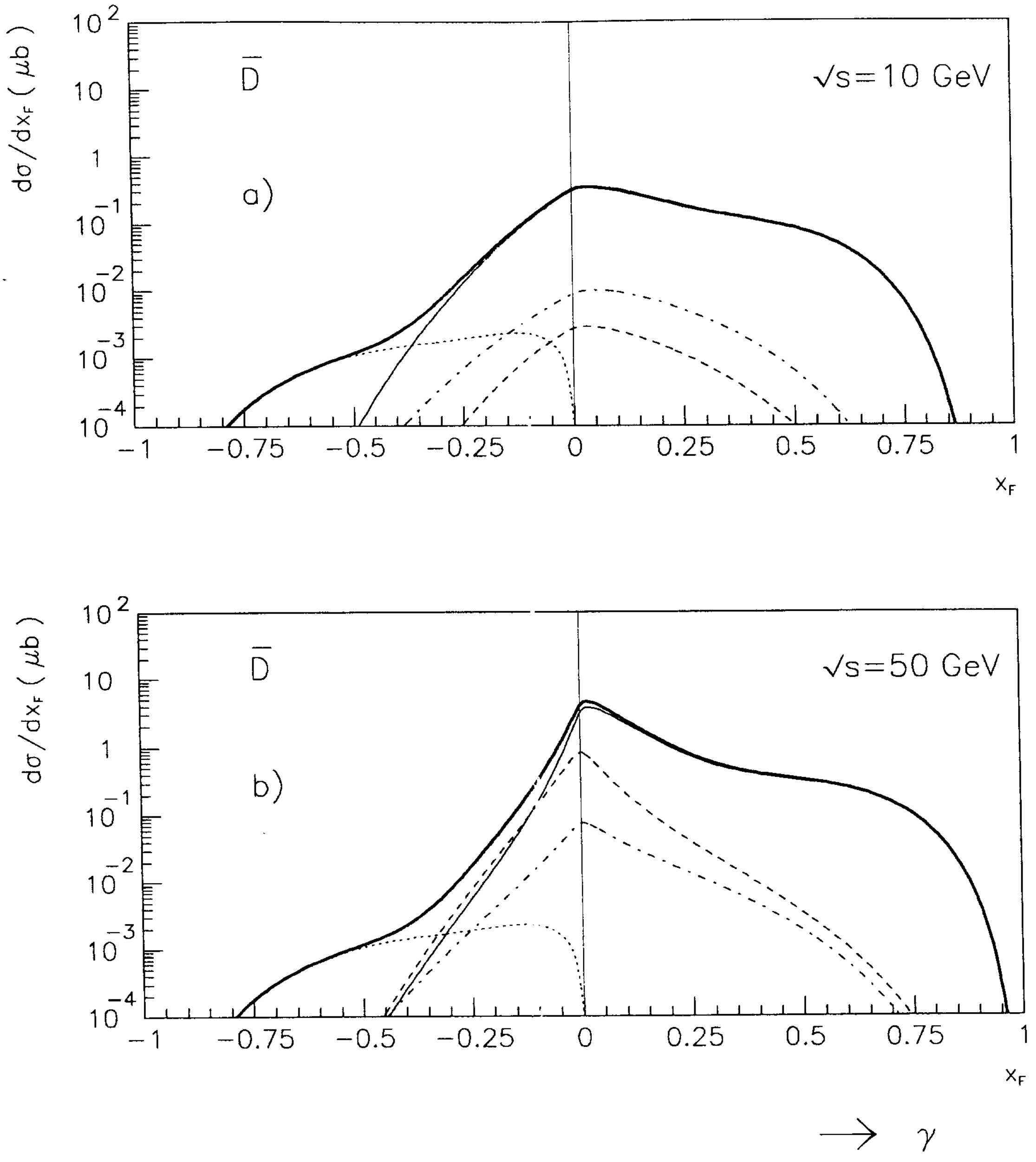

$d\sigma/dx_F$ (μb)
$\bar{D}$
$\sqrt{s}$=10 GeV
a)
x_F
$\bar{D}$
$\sqrt{s}$=50 GeV
b)
x_F
$\longrightarrow \gamma$

Fig. 8a, b

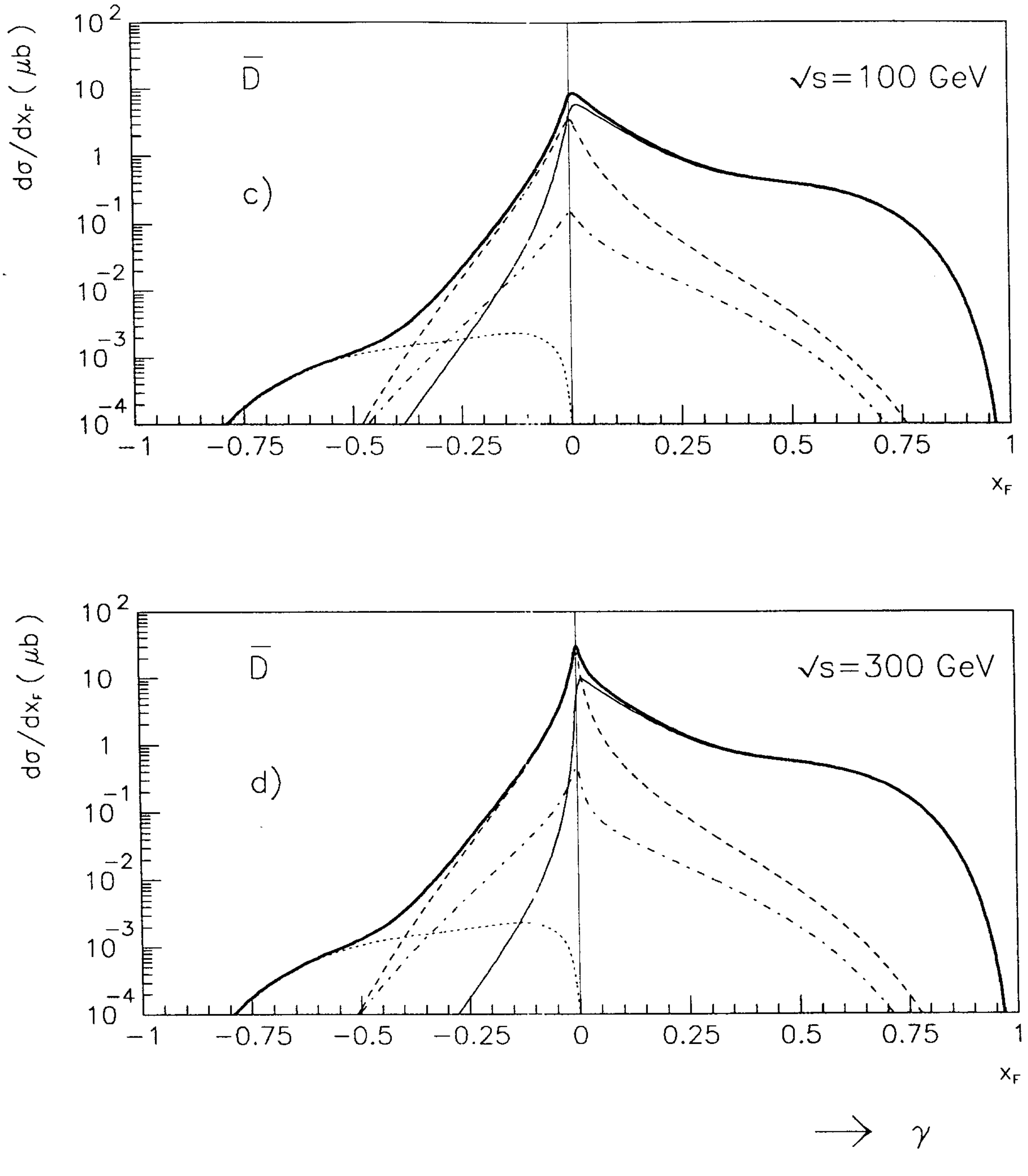
10^2
10
1
10^{-1}
10^{-2}
10^{-3}
10^{-4}
$d\sigma/dx_F$ (μb)
$\bar{D}$
$\sqrt{s}$=100 GeV
c)
−1
−0.75
−0.5
−0.25
0
0.25
0.5
0.75
1
x_F
10^2
10
1
10^{-1}
10^{-2}
10^{-3}
10^{-4}
$d\sigma/dx_F$ (μb)
$\bar{D}$
$\sqrt{s}$=300 GeV
d)
−1
−0.75
−0.5
−0.25
0
0.25
0.5
0.75
1
x_F
$\longrightarrow \gamma$

Fig. 8c, d

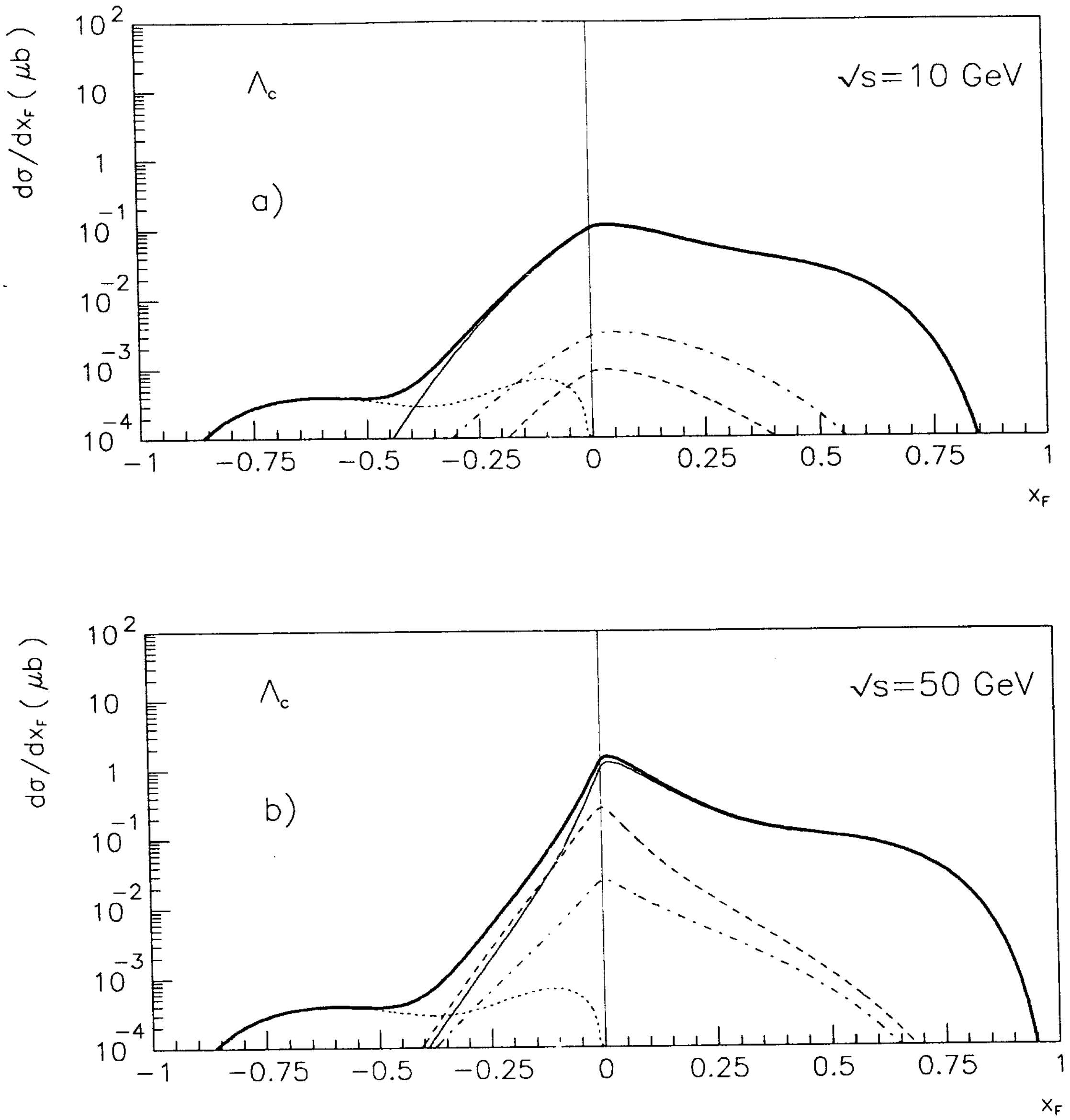

$\rightarrow \gamma$

Fig. 9a, b

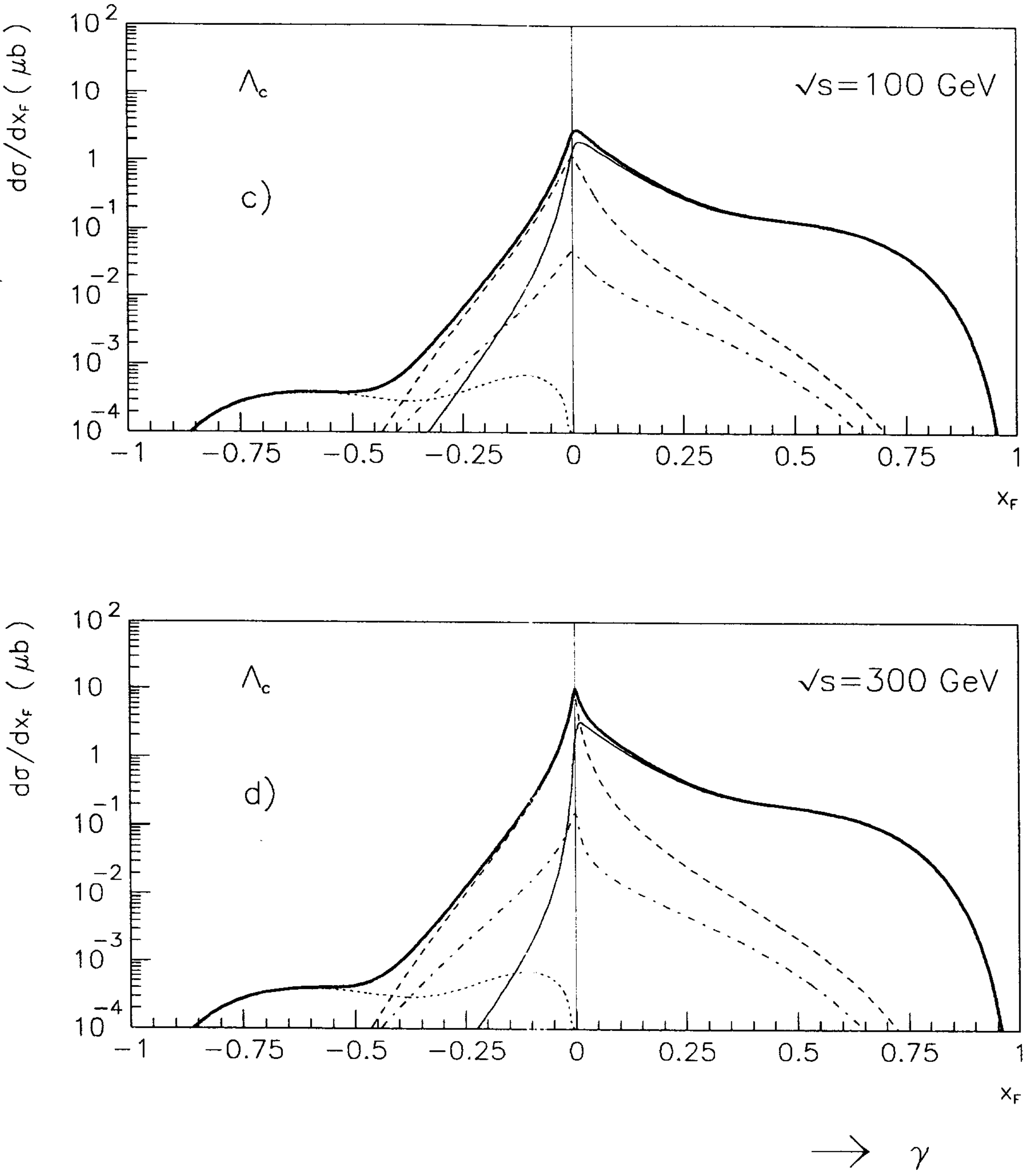

Fig. 9c, d

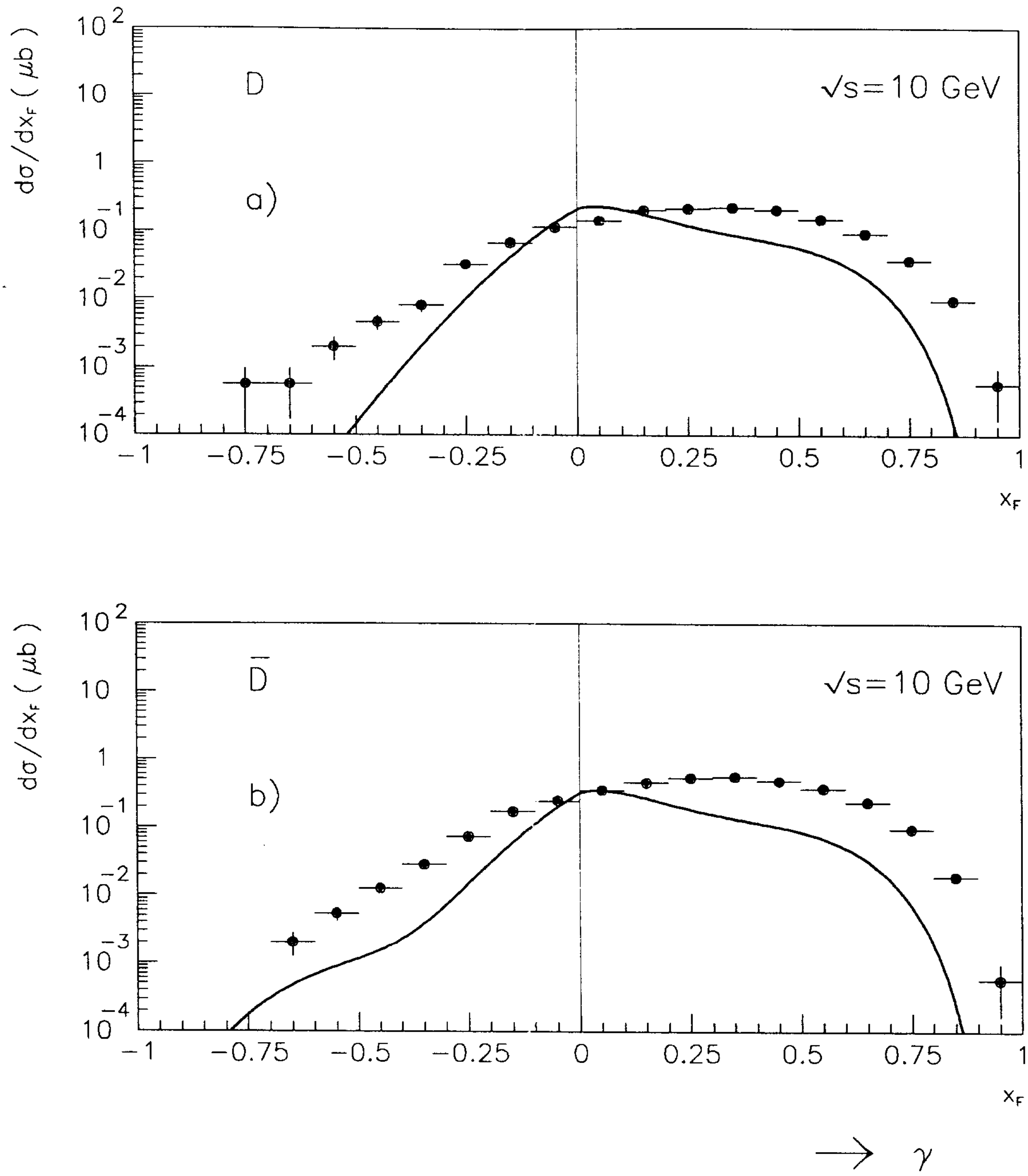

Fig. 10a, b

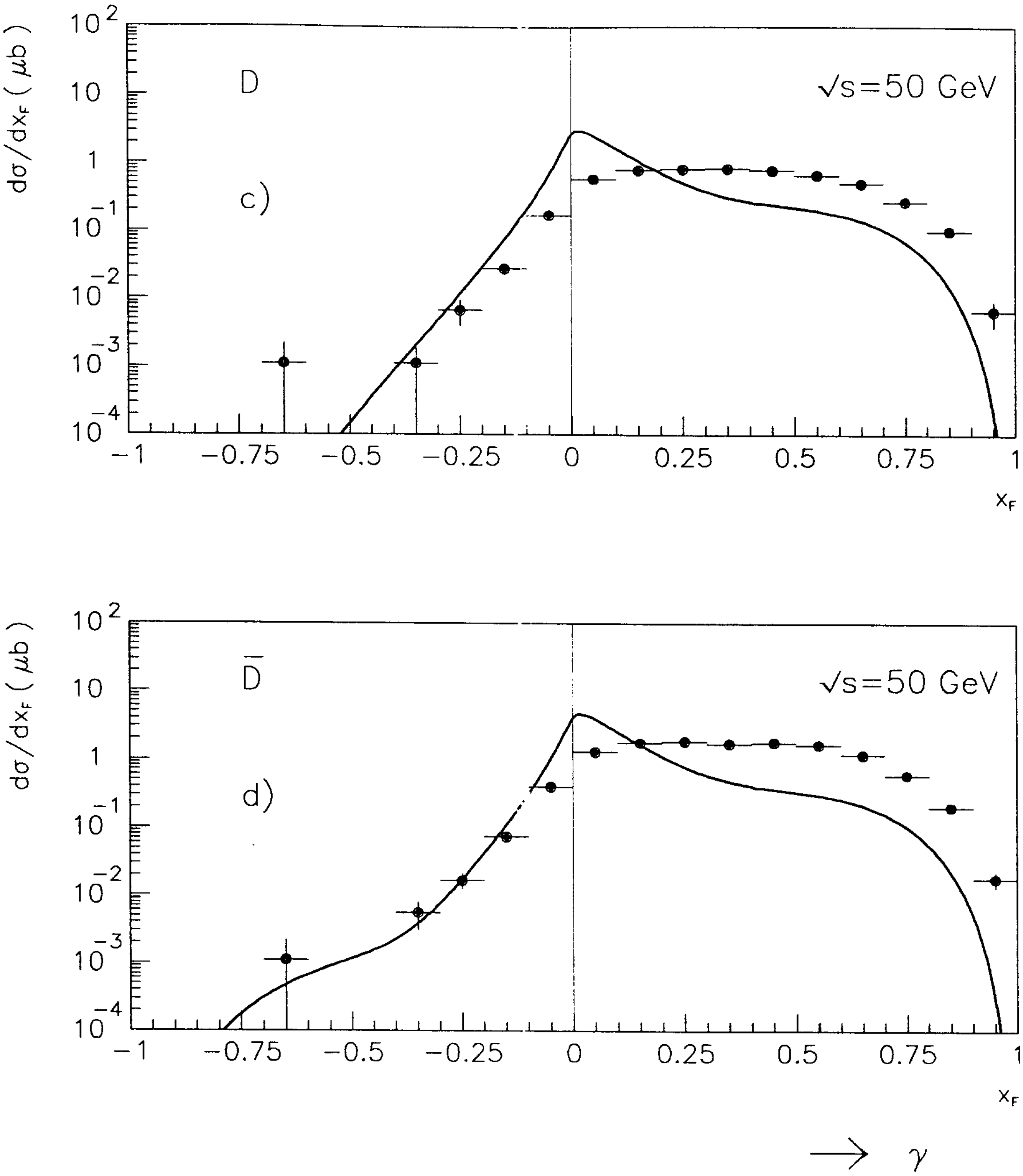

Fig. 10c, d

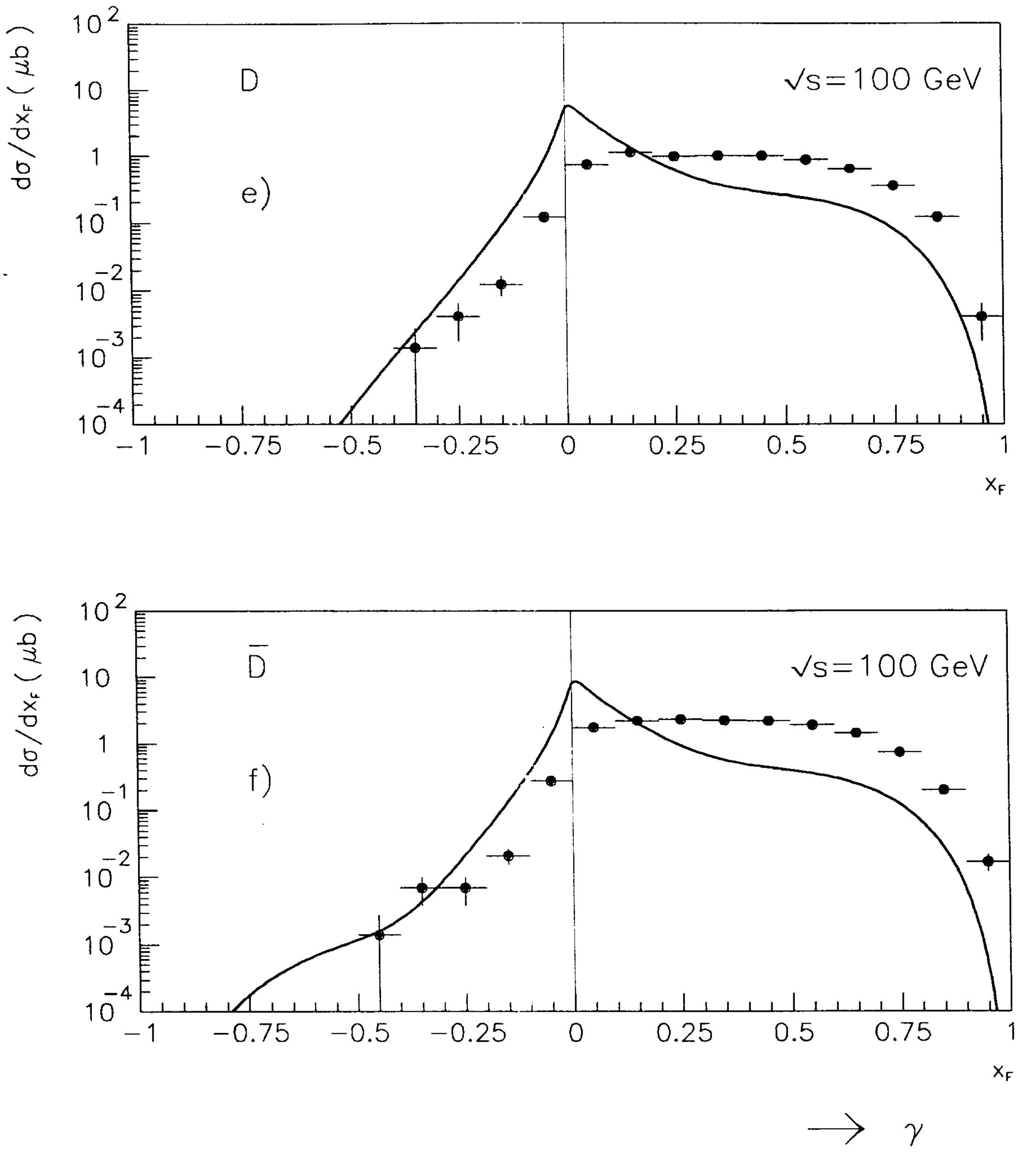

Fig. 10e, f

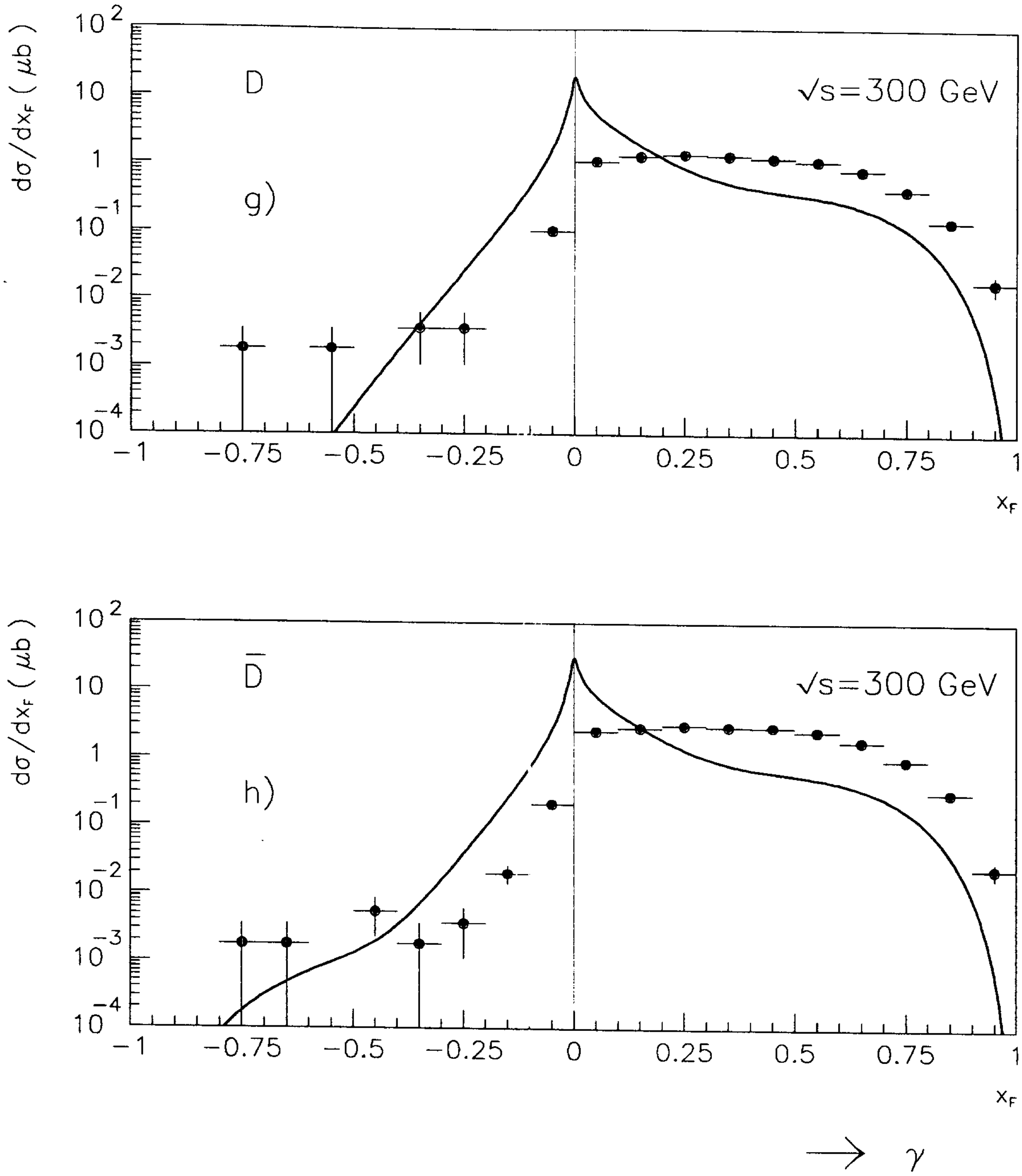

Fig. 10g, h

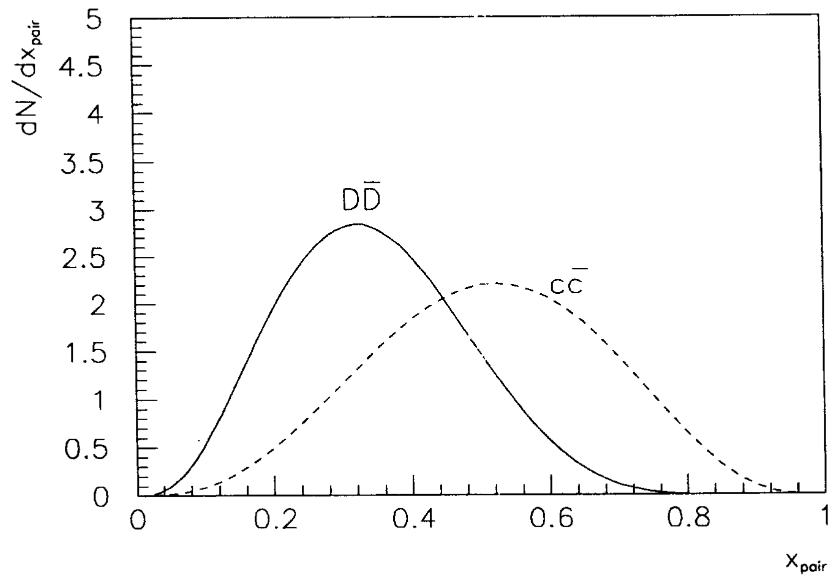

Fig. 11

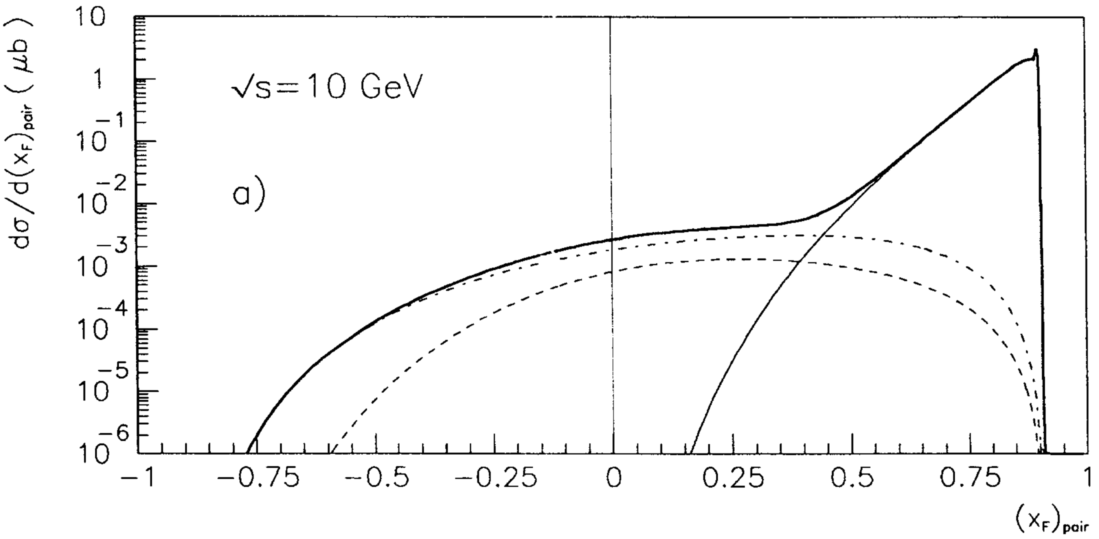

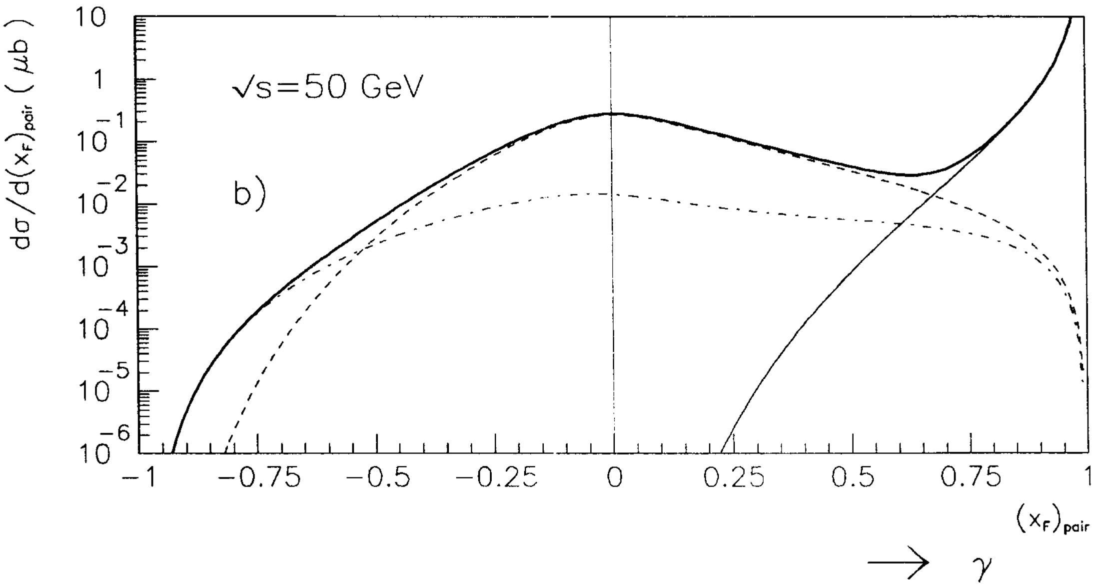

Fig. 12a, b

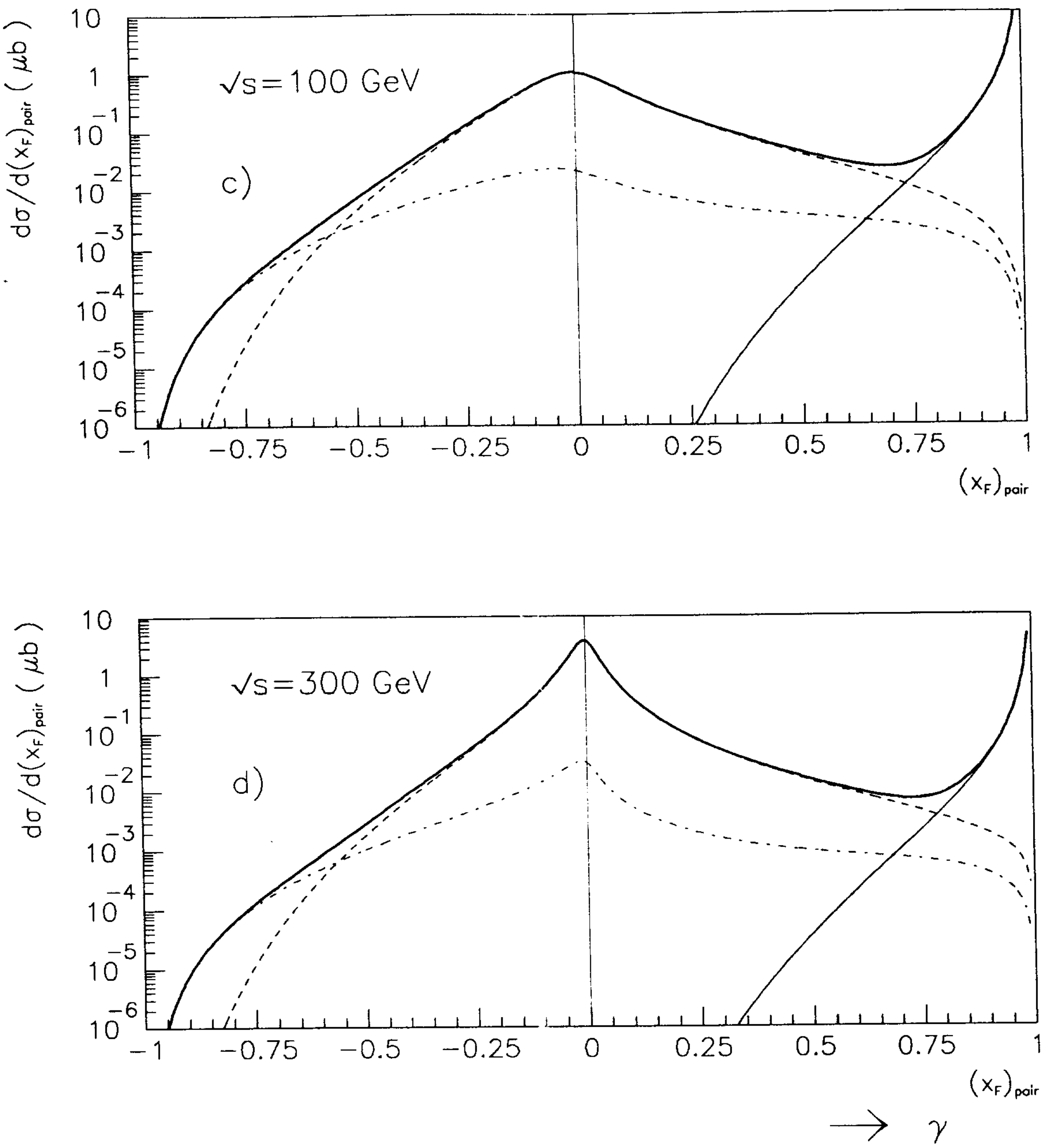

Fig. 12c, d

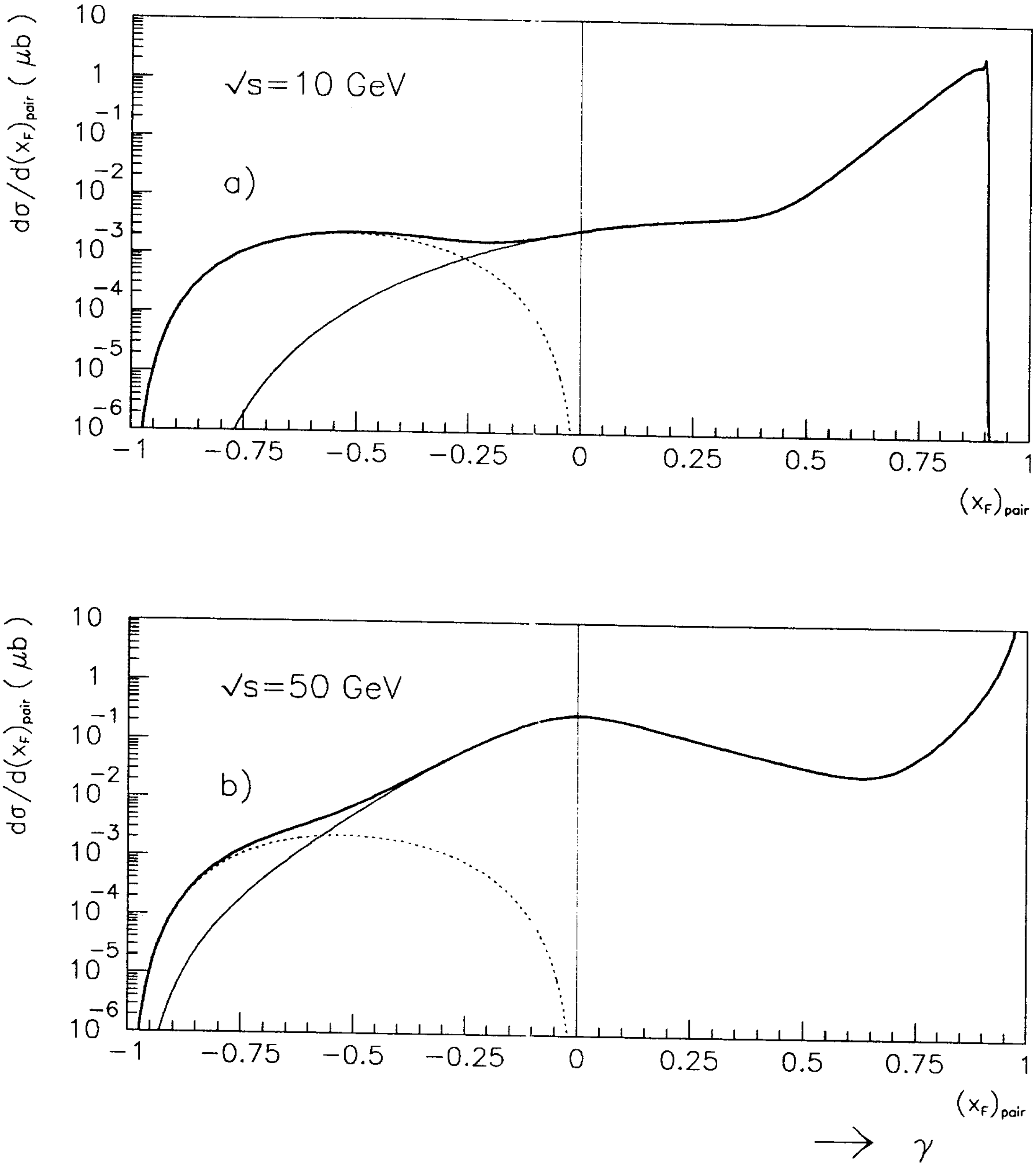

$d\sigma/d(x_F)_{pair}$ (μb)
$\sqrt{s}=10$ GeV
a)
$\sqrt{s}=50$ GeV
b)
10
1
10^{-1}
10^{-2}
10^{-3}
10^{-4}
10^{-5}
10^{-6}
−1
−0.75
−0.5
−0.25
0
0.25
0.5
0.75
1
$(x_F)_{pair}$
$\rightarrow \gamma$

Fig. 13a, b

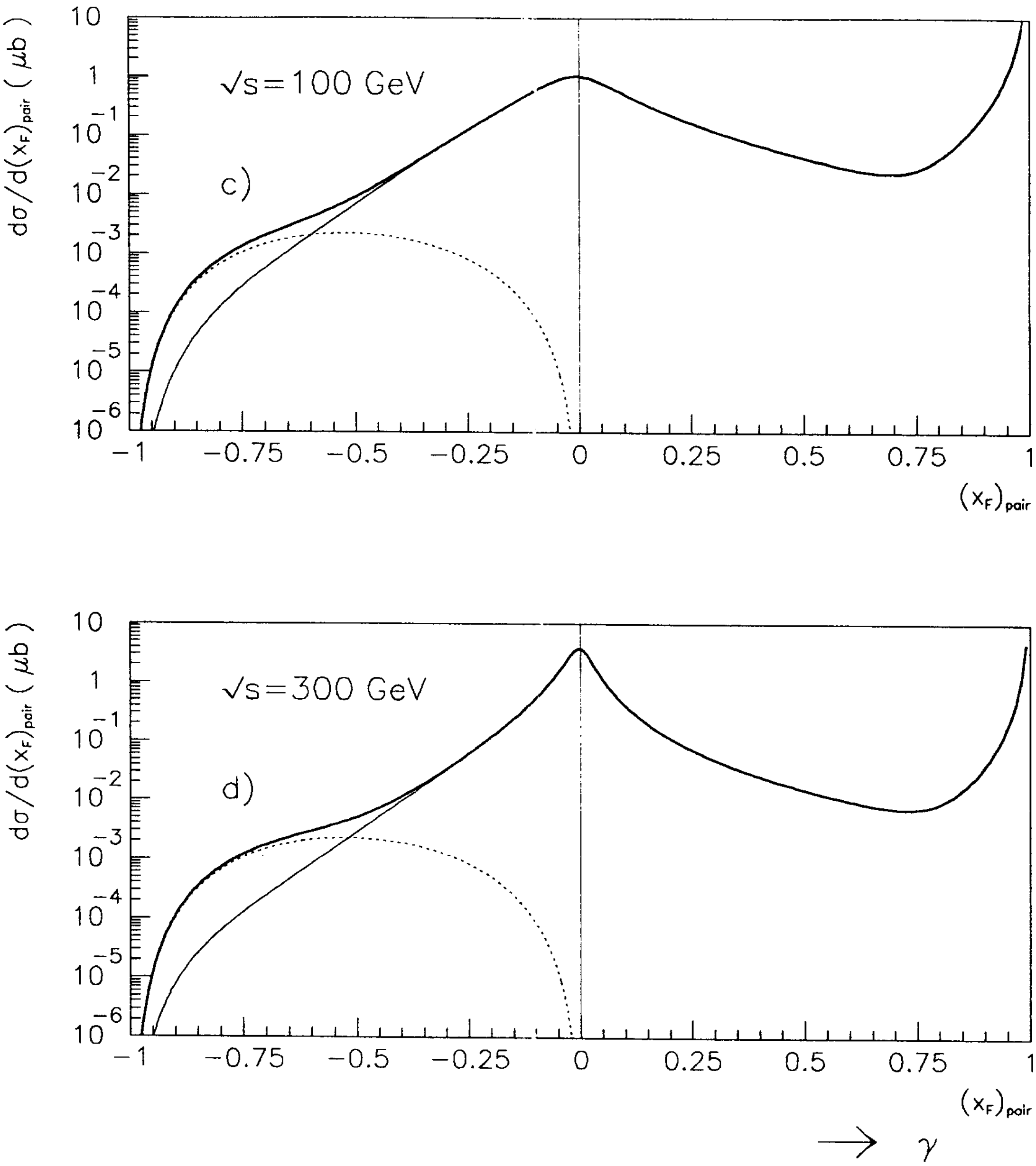

Fig. 13c, d